2004

Investigation Of Ground Penetrating Radar For Detection Of Leaking Pipelines Under Roadway Pavements And Development Of Fiber-Wrapping Repair Technique

Pedro F. Suarez
University of Central Florida

INVESTIGATION OF GROUND PENETRATING RADAR FOR DETECTION OF LEAKING PIPELINES UNDER ROADWAY PAVEMENTS AND DEVELOPMENT OF FIBER-WRAPPING REPAIR TECHNIQUE

by

PEDRO F. SUAREZ
B.S. Instituto Universitario Politecnico de las Fuerzas Armadas Nacionales, 1992

A thesis submitted in partial fulfillment of the requirements
for the degree of Master of Science
in the Department of Civil and Environmental Engineering
in the College of Engineering and Computer Science
at the University of Central Florida
Orlando, Florida

Fall Term
2004

ABSTRACT

Nowadays, it has become a common practice to observe urban roadways undergo severe distress characterized by substantial depressions. In some cases, these pavement depressions are caused by leakages in the connecting joints of sewage pipelines laid beneath the roadway pavement. Manual inspection of pipe leakages has become costly and complex since sewage pipes with relative small diameters do not allow inspection from inside and digging may be required. On the other hand, pipes with large diameters, in which inspection can be made from pipe interior, inspector can not remain inside of the pipe for long periods of time because of toxic fumes.

In order to overcome this problem, a geophysical technique known as ground penetrating radar (GPR) has been proposed as a candidate to detect the leakages. GPR is a nondestructive reflection technique, which uses high frequency electromagnetic waves to acquire subsurface information. GPR contributes to detect leaks in sewer pipes either by detecting underground voids surrounding the faulty pipe, or by detecting anomalies in the depth of the pipe as the radar propagation velocity varies due to the saturation of the soil near the leak.

Once the leakage is detected, on site-repair technique to restore the damaged pipe is not an easy task. In this study, fiber reinforced polymer (FRP) composite created by saturating a fiber sheet with an epoxy resin matrix is proposed to be applied in several layers of overlay to the faulty structure surface. This fiber sheet is typically made of carbon or glass and saturated with the chemical resin matrix and makes the repaired structure even stronger than originally constructed. For the last twenty years, FRP has been used to repair and strengthen concrete

columns by employing a practice known as “fiber wrapping technique”. This method involves the wrapping of unidirectional fiber composite sheets around concrete columns. FRP wrapping approach can be extended to sewage pipelines for repairing and strengthening the distressed pipeline.

The purpose of this study is to detect leakages in sewer pipelines using GPR, and develop an on-site fiber-wrapping technique for repairing and strengthening sewage pipes. In detecting sewer leakages, one case study is presented. The case involves the use of GRP for leakage detection in a sewer pipeline overlaid by flexible pavement that already shows signs of subsidence. Moreover, in developing a repair technique, a gypsum cement mold wrapped with carbon fiber composite material is placed around a large-scale faulty pipe joint, and tested using a MTS servo-controlled hydraulic actuator. In addition, both free ends of the pipes are capped and filled with water to determine the effectiveness of the technique in stopping leaks along the repaired joint.

During the GPR survey performed in the area of study, no clear indications of leakages were observed along the buried sewer pipeline. This lack of traceable signals from the subsurface was the result of the significant attenuation of the radar signal with depth that made impossible to discern effectively any anomaly along the designated pipeline. Although different antennas having center frequencies of 300 and 80 MHz were used and a variety of settings on the GPR unit were tried, the buried pipeline was barely detectable. Nevertheless, signal reflections generated by buried pipelines in other areas such as stormwater pipes on UCF campus and drainage pipelines at road side of University Boulevard were clearly detected, which makes to believe that the significant attenuation of the radar signal at the area of study is due to the

extreme high conductivity of soils which have been severely contaminated by the leakage of sewage from the distressed pipeline.

In contrast, favorable results were obtained in the development of the repair technique since the two-component system, Hydro-stone Gypsum Cement and FRP composite material, wrapped around the faulty joint effectively increased its structural capacity even higher than the pipe original strength.

This thesis is dedicated to my loved wife Mariliana and my treasured son Marco.

My lovely parents,

my beloved sisters,

and, my admired brother.

ACKNOWLEDGEMENTS

I would like to express my sincere gratitude to my advisor, Dr. Shiou-San Kuo, P.E. for his guidance, advice and encouragement not only during the progression of this research but also during the advance of my master.

I also wish to thank Dr. Lei Zhao for his innumerable and valuable comments and for taking the time to review this thesis and Dr Hesham Mahgoub for his support throughout the development of this research; both members of my defense committee. Also, thanks to Mike Olka for his unconditional help during the experimental development at the structure laboratory.

Thanks to CATSS for the funding of this project that made this study possible.

Special thanks to my friends Karishma Desai and Sanjay Shahji for all those Sunday mornings they both kindly dedicated to the completion of this research.

Finally, thanks to my family and friends for their support during the development of this thesis.

TABLE OF CONTENTS

LIST OF TABLES

LIST OF FIGURES

CHAPTER 1

INTRODUCTION

Since the first asphalt roadway appears in the United States in 1870 in Newark, New Jersey, pavement authorities have had the need of searching for models and tools that allow them to develop long and short strategies to keep roads in good conditions and to provide safe journey. Nowadays, urban roadways experience progressive damage characterized by substantial depressions in the pavement surface.

In several cases, pavement depressions are caused by leakages in sewer pipelines laid beneath the pavement. Particular conditions such as poor compaction of pipeline foundation, vertical exciting forces from fluctuated groundwater level, presence of traffic loads exceeding permitted levels, and daily dynamic pressure from sewage flow contribute to the formation of the leakages. These factors either separately or in combination may cause the underground pipe to move when the bottom trench is unstable. Because of pipe rigidity, the joints will also move and gasket compression (plus the joint seal) will be affected. Sufficient joint movement can lead the pipes to separate from each other creating a favorable condition for the leakage to appear. Moreover, the earth load on buried concrete pipes is determined by means of Marston theory, which states that trench walls support part of the weight of the backfill by arch action (Spangler & Handy, 1982). Therefore, an improper compaction of backfill reduces Marston effect making the pipe to support the entirety of the imposed dead loads. Furthermore, if a stress increase on the buried pipe from a surface load, such as a truck wheel, exceeds the rigid pipe's structural limit,

wall failures (cracking) occur and either infiltration or exfiltration take place making the rigid pipe to eventually collapse.

Once the joints crack, the soil around the pipe may be dangerously softened, or even washed away by water forced through the cracks of the pipe (exfiltration) if, because of extraordinary circumstances, the pipe is forced to operate under head. On the other hand, a cracked gravity pipe joint can act as drain, and an excessive amount of groundwater is allowed to infiltrate into the sewer washing the soil surrounding the joints into the pipeline. The loss of soil caused around the pipe joint either by exfiltration or infiltration, in turn, causes the subsidence of road surface.

Many city and county authorities do not address this problem as a leakage problem instead they patch the deteriorated pavement surface repeatedly. This only makes the problem even worse since compaction loads contribute to create additional stresses on the already damaged pipe section. Evaluation of sewer pipe condition requires inspection to determine the infiltration/exfiltration condition. Today, overall indication of pipeline performance is obtained by using variety of techniques such as dye and smoke surveys, air pressure testing, and water tests. Nevertheless, all the mentioned techniques are unfortunately very labor intensive and disruptive. Another technique for pipe condition evaluation currently adopted is the manual survey. Manual inspection in sewer pipes with small diameters involves opening manholes in a progressive manner at periods of low flows and noting any inexplicable clear flows. On the other hand, pipes with large diameters inspection can be made from pipe interior; however, inspector can not remain inside of the pipe for long periods of time because of toxic fumes. Manual surveys are currently the most cost-effective method for tracing infiltration; nevertheless, their

use in exfiltration inspection is very limited and more detailed infiltration of pipelines can be investigated through internal inspections commonly performed through three methods: physical inspection, photographic inspection, and closed-circuit television (CCTV) inspection.

The increasing need for more reliable data during condition assessment of sewer pipelines is striving governmental authorities to look for enhanced alternatives. One of the most promising non-destructive techniques may be the use of the Ground Penetrating Radar (GPR) survey. GPR is a geophysical method that uses high frequency pulsed electromagnetic waves (typically from 10 MHz to 1.5 GHz or higher) to acquire subsurface information. The electromagnetic waves are propagated downward into the ground until these waves meet geological targets or different objects. Then the propagating waves are reflected back and recorded on a digital storage device as they hit the ground surface for later interpretation. The radar reflection behavior depends on the contrast in the electrical and magnetic properties of the material the electromagnetic waves are traveling through. GPR contributes to detect leaks in sewer pipes either by detecting underground voids surrounding the fractured pipe, or by detecting anomalies in the depth of the pipe as the radar propagation velocity varies due to the saturation of the soil near the leak. A leak detection survey was performed using GPR in a sewer pipeline overlaid by flexible pavement that already shows signs of subsidence on University Boulevard westbound near the intersection of University Boulevard and Rouse Road.

On-site repair technique without replacing the joint connectors is not an easy task. Fiber Reinforced Polymers (FRP) is a composite material that consists of continuous reinforcing fibers held together by surrounding polymer binder. The fibers bear the structural loads and the polymer, also called the matrix; transfer the load from fiber to fiber. The orientation and

mechanical properties of the fibers along with the matrix properties determine the mechanical response characteristics of the whole, and are predicted by a developed theory model called classical laminate theory. FRP is used increasingly in high-performance applications that require high specific strength and/or stiffness, low electrical conductivity, transparency to radio emissions, and resistance to corrosion. As it is known, lateral confinement of concrete increases its strength and ductility. Therefore, confining of concrete columns is advantageous for strengthening and repairing existing columns. For the last twenty years FRP have been used to strength and repair damaged columns in bridge structures using the so-called “fiber wrapping technique”, characterized by the wrapping of unidirectional fiber composites sheets around concrete columns (Saadatmanesh, Ehsani, & Li, 1994). The relevance of the fiber wrapping approach to concrete pipelines is first proposed in this study, which is intended to repair and strengthen the distressed or cracked pipelines.

In developing a repair technique, large-scale concrete pipes were assembled. The rubber gasket in the joint was intentionally withdrawn and the spigot end was pulled back from its customary position inside the bell to recreate a faulty joint. Then a gypsum cement rim was designed and built around the faulty joint and then wrapped with carbon fiber reinforced polymers. Subsequently a vertical force, normal to the longitudinal axis of the pipes, was applied to determine the structural capability of the strengthened joint in resisting the shear force induced by the test force. In addition, both free ends of the pipes were capped and filled with water to determine the effectiveness of the repair technique to prevent leakages.

Objective of Research

Two main objectives of this study were:

1) To detect leakages in pipe joints using Ground Penetrating Radar (GPR).
2) To develop an on-site fiber wrapping technique for repairing and strengthening of underground sewage pipes.

Format of Thesis

The thesis consists of five chapters, as follows:

- Chapter 1 presents an introduction of the study giving to the reader and overview of the study.
- Chapter 2 is a review of previous research on detection of leakages using GPR and the use of FRP in repairing and strengthening pipes. This chapter also provides a theoretical background of GPR as well as FRP fundamentals. Finally a broad discussion regarding the loads on underground conduits is presented.
- Chapter 3 reports a valuable description of methods and formulas used in the computation of loads on buried concrete pipes.
- Chapter 4 provides a complete description of the GPR survey performed in the detection of leakages as well as the experimental work involved in the development of the wrapping repair technique, including description of materials, preparation of specimens, test procedure and test observations.
- Chapter 5 provides an extensive discussion of test results.

- Chapter 6 offers conclusions and lists a number of recommendations to consider in further work related to this research.

CHAPTER 2

LITERATURE REVIEW AND ADDITIONAL INFORMATION

Detection of Leakages in Pipe Joints using Ground Penetrating Radar

The presence of leakages in sewer systems characterized either by an infiltration or exfiltration condition represents a mayor problem to be addressed by city officials and D.O.T. pavement engineers. Considerable volumes of ground water infiltration greatly increase the costs incurred due to over design of the sewer pipeline and additional wastewater treatment. Moreover, as infiltration water enters the pipe, the soil surrounding the leakage area is washed into the pipe creating underground voids that eventually provoke the subsidence of pavement system causing traffic disruption, damage to vehicles, and in some cases, if the pavement suddenly collapses even loss of life. On the other hand, in pressurized sewage pipes water forced though the cracks of the pipe at the leakage zone represents a serious environmental problem.

The idea of developing a non-disruptive, capital cost effective, and accurate technique to assess the sewer pipeline condition in terms of leakages has in recent years caught the attention of numerous researchers. Variety of techniques, some of them still in the development stage, is being used in the detection of pipeline leakage and detection of cavities. Ground Penetrating Radar (GPR) represents one of the most promising new inspection techniques in providing details of pipe position, existence of soil voids and areas with water leakage (Eiswirth, Heske, Burn, & DeSilva, 2001).

Several preceding studies demonstrate the feasibility of GPR survey in detecting buried objects, including pipelines. Moreover, previous studies have been also conducted, sometimes in

conjunction with other methods, to recognize the existence of leakages in buried pipelines. Fred Graf (1989) illustrated direct GPR detection of gas pipeline leaks developing a technique based on the GPR's ability of showing an apparent pipe rise in elevation in the leakage zone. The very dry natural gas (at a dew point of -41 ºC) leaking into the soil caused the pulse signal to speed up in the drier soil area. This increase in the velocity of the radar pulse provokes the GPR to reflect a chance in elevation in the leaking area reported as a 'bump" in the GPR profile. Powers and Olhoeft (1997) in their study "Modeling the GPR Response of leaking buried pipes", they compared synthetic GPR signatures for leaking and nonleaking pipes with various configurations

Recently, special attention has been taken into water distribution systems where a significant percentage of water is lost due to leakage from distribution pipes. Osama and Giamou (1998) conducted an extensive leak detection survey using ground penetrating radar to evaluate its potential for leak detection. The survey was performed at a specially built leak detection experimental site, where a plastic pipeline was buried in a soft silty clay soil and several types of leakages were intentionally created under controlled conditions. The facility has a 200 m long PVC pipe, 150 mm in diameter and buried at a depth of 2.4 m. During the survey the maximum penetration of the radar signals was between 2 to 3 m. Radar profiles from the leak site illustrated an apparent difference in depth among different sections of the same pipeline. In the profiles taken above the leakage area the pipe appeared slightly deeper than in the ones taken away from it. The apparent differences in depth were attributed to a slow-down in the radar wave due to the presence of moisture in the soil near the leakage.

A series of laboratory experiments have been conducted at the University of Arkansas (Eyuboglu, Mahdi, & Al-Shukri, 2003) to determine the validity and effectiveness of GPR

technology in detecting water leakage in plastic and metal pipes. In achieving the purpose of the study a wooden boxed was constructed and filled with sand in which a plastic pipe and later a metal pipe were buried in separate experiments to simulate leaks. Both pipes were previously perforated in the middle and one of their ends connected to a hose for water injection. Plastic PVC pipe and metal pipe were buried in the sand at a depth of 18 and 20 cm, respectively. Once water was injected to simulate a leak numerous GPR profiles were collected for different combinations of survey direction, radiation pattern, pipe types, and amount of injected water. Results obtained from this study illustrated how effective GPR is in the detection of leaks. Besides, an outdoor test bed is currently under construction in collaboration with Central Arkansas Water (CAW) to simulate a large-scale leaking water distribution system and its detection using the GPR technique

Eiswirth et al. (2001) note the effectiveness of the GPR technique in detecting leaks in pipes and providing information of soil conditions around pipelines; however, they recognize that data interpretation requires substantial experience and training because the radar output is very difficult to interpret. In addition, Dr. Kuo has conducted numerous applications of using GPR for subsurface detection of sinkholes in Florida (1985); soil strata (1984); buried drums and soil contamination (1986); and others at the University of Central Florida since 1982.

Theoretical Background of GPR

Ground penetrating radar (GPR) is a geophysical, non-destructive method that has been developed over the past thirty years for high resolution, subsurface investigations. GPR produces high frequency pulsed electromagnetic waves (generally 10 MHz to 1.5 GHz) that travel through

the ground until these waves meet geological targets or different objects then they reflect to the surface. The function of GPR wave transmission and reflection is shown in Figure 1.

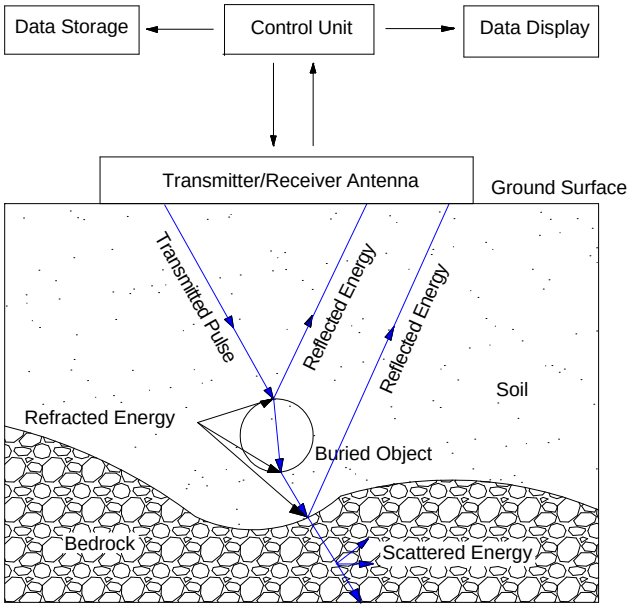

Figure 1: Functional Diagram of GPR Equipment
Source: Ground Penetrating Radar. Field Analytic Technologies Encyclopedia. U.S. Environmental Protection Agency, 2003

As radar pulses are transmitted through various materials on their way to the buried target feature, their velocity changes depending basically on two primary electrical properties of the subsurface: electrical resistivity and dielectric constant. Reflections are produced by changes in the dielectric constant due to changes in the subsurface material (Eyuboglu et al., 2003). The greater the contrast between two materials at a subsurface interface, the stronger the reflected signal, resulting in a higher amplitude reflected wave. Such contrasts where reflections occur are usually created by changes in electrical properties of the sediment or soil, variations in water

content, lithologic changes, or changes in bulk density at stratigraphic interfaces. Void spaces in the ground or buried pipes or conduits will also generate strong radar reflections due to a significant change in radar-wave velocity (Conyers, Ernenwein, & Bedal, 2002)

The penetration capabilities of GPR are dependent of the electrical conductivity and moisture content of soil investigated and the frequency of the antenna used. In materials with high conductivity such as clayey soil, radar waves attenuate (in the form of absorption or dispersion) drastically reducing the penetration depth. Loose soil and high moisture contents greatly increase both the conductivity and dielectric constant, and thus decreases the propagation of the penetrating signals. Moreover, high frequency waves produce higher resolution models at shallow depth only, whereas low frequency waves produce lower resolution models that may be located at greater depths. When using high frequency antennas (500 MHz – 1.5 GHz), penetration depth reaches 3 to 10 feet; while using low frequency antennas (80 – 300 MHz) penetration depth can reach 15 to 60 feet. Thus, proper selection of antenna is based on the nature of target of study and the objective depth.

Radar antennas are moved along the ground in linear transects while two-dimensional profiles of a large number of periodic reflections are created, producing a profile of subsurface stratigraphy and buried features along each line. To produce these reflection profiles the two-way travel time and the amplitude and wavelength of the reflected radar waves are then amplified, processed, and recorded for immediate viewing or later post-acquisition processing and display. When data are acquired in a series of transects within a grid, and the reflections are correlated and processed, an accurate three-dimensional picture of buried features and associated stratigraphy can be constructed (Conyers et al., 2002).

As mentioned before the success of the GPR technique resides in the ability of the various materials in allow or prevent the transmission of radar waves. In calculating depth of penetration, the two-way travel time and propagation velocity of the radar signal must be known. The two-time travel time can be determined from the graphic representation of the reflected radar signals. The propagation velocity of the radar signal can be calculated by Equation 1 as follow:

$$v = \frac{c}{\sqrt{e_r}} = \frac{0.3}{\sqrt{e_r}} m/ns \quad (1)$$

where v is the average propagation velocity of the signal (nsec/feet), e_r is the dielectric constant of the material (unitless), and c is the velocity of light (˜ 1 foot/nsec).

Geophysical Surveys Systems, Inc. in its SIRveyor SIR-20 User's Manual 2002 tabulates dielectric constants for common materials. Those dielectric constants have been transcribed in Table 1. Subsequently, the depth of penetration can be determined using Equation 2 as follow:

$$D = \frac{t \times v}{2} \quad (2)$$

where D is the depth of penetration (feet) and t is the two-way travel time (nsec).

When information about subsurface is not available or the material is suspected not to be homogeneous, the dielectric constant of the material can be precisely calculated knowing the depth of an object immerse in the same material and the two-way travel time.

Table 1 Dielectric Value for Common Materials

Material	Dielectric Constant	Velocity (mm/ns)
Air	1	300
Water (fresh)	81	33
Water (sea)	81	33
Polar snow	1.4 – 3	194 – 252
Polar Ice	3 – 3.15	168
Sand (dry)	3 – 6	120 – 170
Sand (wet)	25 – 30	55 – 60
Silt (wet)	10	95
Clay (wet)	8 – 15	86 – 110
Clay soil (dry)	3	173
Agricultural land	15	77
“Average soil”	16	75
Limestone	7 – 9	100 – 113
Sandstone (wet)	6	112
Concrete	6 – 8	55 – 112
Asphalt	3 – 5	134 – 173
PVC	3	173

Source: SIRveyor SIR-20 User’s Manual, 2002.

Developing of a Fiber-Wrapping Technique to Repair and Strengthening Pipe Joints

One of the worst scenarios for any city utility officials and D.O.T. pavement engineers is the failure in one its pipelines under the pavement. The cost of repairs represents just part of the problem. Once the repair process takes into effect also jumbled traffic and neighbor disruptions are present. As a result, new non-disruptive repair techniques are being developed in order to avoid those inconvenient scenarios.

Nowadays, the idea of strengthening existent pipes with FRP has gained some interest in the construction industry since the application of composite materials (FRP) reduces or eliminates facility shutdown and loss of revenue, reduces the amount of labor needed, requires no heavy and sophisticated equipment and causes no significant loss of facility space compared with traditional methods.

There are several documented experiences such as the Cranston's water line rehabilitation in Rhode Island and the Paloverde Nuclear Generating Station, in which concrete pipes were strengthened wrapping FRP around the damaged pipe. In both of this reported experiences the pipes were large –diameter prestressed concrete cylinder pipes (PCCP) used to carry water and sewer. The PCCP are constructed from steel and concrete, including high strength steel wires that are prestressed in the hook direction. Corrosion of steel reinforcement represents a big issue in PCCP causing them to fail and eventually collapse. The FRP has always been wrapped internally around the circumference of the pipe.

The providence water supply Board faced an immense problem when a mayor section of a 102 inch-diameter water line in Cranston, Rhode Island failed completely. The cause of the pipe collapse was the rupture of the prestressing wire due to corrosion. In addition, after a

rigorous inspection of the pipeline using ultrasonic (pulse echo) and acoustic (hammer sounding) testing, vulnerabilities were detected in twenty nonconsecutive 16-foot-long sections within a five-mile stretch of the pipeline. Traditional methods suggested the insertion of a steel liner in sections, welding them together, and then grouting the annular space between the new and old section. The traditional procedure implied significant excavation with long periods of downtime. SPS, a national concrete repair contractor, proposed the installation of a carbon fiber-reinforced polymer (FRP) sheet lining as the fastest, least disruptive, and most-cost effective repair solution (Thomas & St. John, 2003). The pipe's interior was waterblasting removing any sediment from the surface. To prepare the surface, an epoxy primer was applied, followed by a trowel-applied epoxy to fill voids and level irregularities. FRP layers were internally wrapped around the circumference of the pipe, as well as longitudinally, building basically a pipe within a pipe. Workers used scaffolding to reach the top of the pipe and avoid walking on the bottom. Metal rib rollers were used to push out any air trapped in between the FRP and pipe surface, and to press the FRP sheets into the saturant. A second layer of resin was then applied to form a complete fiber/laminate matrix. To avoid water infiltrating behind the FRP system, a waterstop-type termination was projected for the end of each 16-foot section of pipe. By using FRP, Providence Water Supply did not have to dig, replace, or lining long pipe sections.

Quakewrap, Inc., a leading designer, supplier, and installer of FRP, located in Tucson, Arizona; has developed a repair technique for concrete pipes named PipeWrap^{TM} system, which adds a tremendous strength to any pipe to be repaired, restoring hoop and longitudinal strength and it is also capable of stopping leaks. The PipeWrap ^{TM} system consists of a multi-ply system in which saturated carbon fabrics are installed on top of one another to the interior surface of

large-diameter pipes. Among the experiences of PipeWrap^{TM}, the Paloverde Nuclear Generating Station is one of them. In a number of prestressed circular concrete pipes (PCCP) in this facility, cracks were present due to the corrosion of steel wires causing the weakening of the pipes. Quakewrap Inc designed a special fabric capable of providing enough strength, which reduced the number of wraps in the pipe to three layers. Before the FRP was applied, the proposed design was tested. A similar PCCP was intentionally weakened and wrapped with PipeWrap^{TM}, its ends were capped with steel plates and the pipe was pressurized. Testing was stopped when the pipe pressure exceeded the original design strength of the pipe. The installation began with the application of a primer, QuakeBond J100WP, to the interior surface of the pipes. Secondly, a tack coat, QuakeBond J200TC, was applied to the primed interior surface to fill voids and level imperfections. The tack coat J200TC also has an immediate high tack consistency, allowing it to hold the saturated FRP layer in place during cure, especially in overhead surfaces. Then, the saturated fabric was applied taking care of edges and overlaps, which were carefully finished. Because of the presence of chemicals in the water to flow along the restored pipes, two layers of High Chemical Resistant Coating, J400HCR, were applied to protect the PipeWrapTM system.

Recently, other composite materials have been developed and are commercially available for remedial repairs to defects and anomalies in pipelines. One of them, Synto-Glass^{R}, a fiberglass cloth impregnated with a resin that is activated by salt or fresh water is especially suitable for reinforcement of corroded pipelines and repairing leaking pipes, flanges, joints and fittings. Nevertheless, SyntoGlass is restrained to pipes smaller than 48 inches.

Fiber Reinforced Polymer Composites

Fiber-reinforced polymeric composites, FRP, are materials that consist of continuous reinforcing fibers held together by a surrounding resin binder as shown in Figure 2. The fibers provide increased stiffness and tensile capacity. The resin offers high compressive strength and binds the fiber into a firm matrix (Tang, 1997). The orientation and mechanical properties of the fibers along with the matrix properties determine the mechanical response characteristics of the whole, and are predicted by a developed theory model called classical laminate theory.

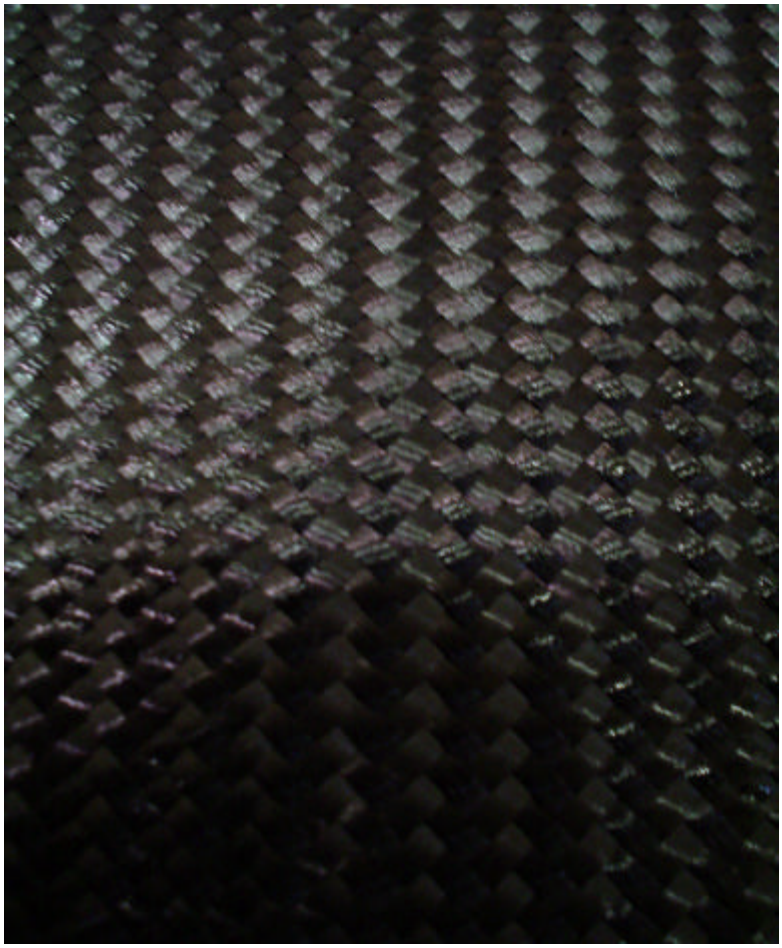

Figure 2: Carbon Fiber Reinforced Polymers.

Benefits of fiber-reinforced polymer composites for structural applications are their high compressive, tensile, and flexural strength. Another benefit of FRP composites is the lightweight of the material. In general, FRP weigh one-fifteenth the weight of steel. In addition to these properties, through the use of fillers and additives, composites can fight against chemical reactions, inhibit ultraviolet rays, and have low water absorption

The most common fiber materials used in polymeric composites are glass, carbon, and aramid. Carbon fiber offers exceptional strength and stiffness. The tensile stress-strain curve is linear to the point of rupture. The material also has a very high fatigue and creep resistance.

For the last twenty years, thermal setting resins and fiber rods and sheets are being used to repair and upgrade structural systems. FRP composites are being used to repair and strengthen concrete columns by employing a practice known as “fiber wrapping technique” (Pico, 1997). This method involves the wrapping of unidirectional fiber composite sheets around concrete columns promoting the lateral confinement of concrete, which enhances the strength and ductility of the existent column. Research conducted at the University of California at San Diego (UCSD) determined that wrapping reinforced concrete columns with FRP not only provided an increase in axial or vertical load capacity of the column and enhanced its ductility but also provided a significant increase in shear strength and inhibited rebar lap splice failure, a common scenario in seismic events (Watson, 2000). Testing performed at the Georgia Department of Transportation Laboratories has determined that standard concrete cylinders wrapped with glass FRP increased their axial capacity by 135 percent.

CHAPTER 3

LOADS ON UNDERGROUND CONCRETE PIPES

In order to determine the magnitude of the load applied on concrete pipes installed underneath flexible pavements, both overlying earth material (overburden) and traffic loads should be computed. Considerations and procedures for calculating earth and traffic loads are further presented.

Determination of Earth Load

The Marston Theory is largely applied in calculating the earth load imposed by the weight of the soil column above the buried pipe, (Spangler & Handy, 1982). The Marston theory affirms that the load of the soil column above a buried pipe is modified by arch action, in which part of the weight of the prism of soil immediately above the pipe is transferred to the adjacent side prisms, relieving the pipe of some of its soil burden. Or in other cases due to an invert arch action the load on the pipe is increased since additional load from the side prisms is transferred to the prism of soil directly above the pipe.

In the application of the Marston Theory the manner in which the pipe is installed is critical in computing the load over the pipe. For load calculation purposes, buried concrete pipes can be divided into four major categories, known as ditch pipes, positive projective pipes, negative projective pipes, and jacked or tunneled pipes as seen in Figure 3. Since sewer concrete pipes are conventionally installed as trench and positive and negative projecting pipes no reference is made regarding jacked pipes in this research. Most likely, the trench or negative

projecting installation may be appropriate for the construction of the pipeline under the pavement.

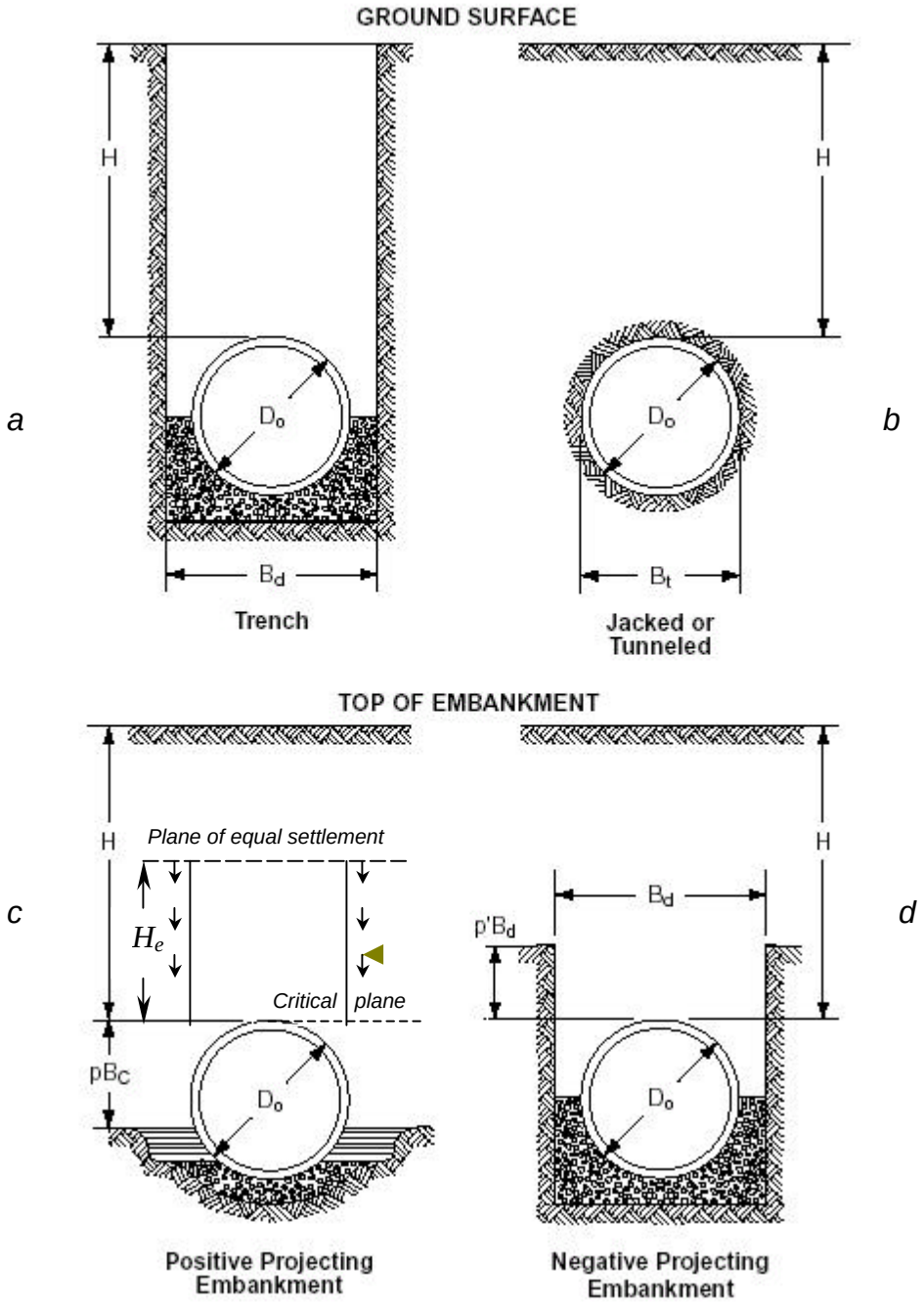

Figure 3: Various classes of pipe installations
Source: Concrete Pipe Design Manual 2000. American Concrete Pipe Association.

Ditch Pipes

In the case of ditch or trench pipes, the pipe is installed in a relatively narrow ditch dug in undisturbed soil and which is then covered by earth backfill. In trench pipes the backfilling material tends to settle downward, which in combination with the settlement of the pipe into its soil foundation causes the prism of soil within the ditch and above the pipe to move downward relative to the undisturbed soil at the sides. This relative movement creates shearing stresses or friction forces along the sides of the ditch that act upward in direction. The combination of these friction forces with horizontal forces creates an arch effect that relieves the pipe from part of the weight of the soil prism above it.

In a trench condition the load of the backfill on the pipe is computed by Equation 3 (Spangler & Handy, 1982).

$$W_c = C_d g B_d^{\,2} \tag{3}$$

where W_c is the load on conduit, in newtons per meter (lb/linear ft), *?* is the unit weight (wet density) of filling material, in newtons per cubic meter (lb/ft^3), and B_d is the horizontal width of the ditch at top of conduit, in meters (ft). C_d represents the load coefficient for ditch conduits and can be calculated using Equation 4.

$$C_d = \frac{1 - e^{-2Km'(H/B_d')}}{2Km'} \tag{4}$$

where *K* is the ratio of active lateral unit pressure to vertical unit pressure (Rankine's ratio) and *μ'* is the coefficient of friction between fill material and sides of ditch. Typical values of *Ku'* are:

$K\mu'$ = .1924 Max. for granular materials without cohesion

$K\mu'$ = .165 Max. for sand and gravel

$K\mu'$ = .150 Max. for saturated top soil

$K\mu'$ = .130 Max. for ordinary clay

$K\mu'$ = .110 Max for saturated clay

Positive Projecting Pipes

Positive projecting pipes are installed in shallow bedding with its top projecting over the original ground or compacted fill and then covered with an embankment. In this type of pipe installation the vertical distance from the natural ground surface or compacted fill to the top of the pipe is represented by *pBc*, where p is the projection ratio as shown in Figure 3 drawing (c).

In concrete pipes installed as positive projecting pipes, during and after construction the side soil prisms tend to settle downward with respect to the interior prism above the pipe. The shearing forces on the interior prism are directed downward causing the pipe to support a load even greater than the simple weight of the soil prism immediately above it.

The magnitude and the resultant movement in between the interior soil prism (immediately above the concrete pipe) and the adjacent exterior prisms are influenced by the settlement of certain elements of the pipe and the adjacent soil. For the interior prism of soil (above the pipe) the elements involved are the settlement of the pipe into its foundation and the shortening of the vertical height of the pipe. Likewise, the compression strain of the side

columns of soil and settlement of the natural ground surface adjacent to the conduit represent the elements involved in the movement of the adjacent exterior prisms. These settlements are related to each other into an abstract ratio known as the settlement ratio. Values of settlement ratios from observations of the performance of actual pipes under embankments are shown in Table 2.

Table 2 Values of Settlement Ratio

Conditions	Settlement Ratio
Rigid culvert on foundation of rock or unyielding soil	+1.0
Rigid culvert on foundation of ordinary soil	+0.5 - +0.8
Rigid culvert on foundation of material that yields with respect to adjacent natural ground	0 - +0.5

Source: Soil Engineering. Spangler & Handy, 1982.

In connection with the settlement of the pipe and the prism of soil adjacent to it, another term to be defined is the horizontal plane through the top of the pipe when the fill is level with its top known as the critical plane as shown in Figure 3 drawing (c). In concrete pipes the critical plane tends to settle more than the top of the pipe; therefore the exterior prisms move downward with respect to the prism of soil above the pipe, behavior characteristic of the projection condition in rigid pipes.

Another feature characteristic of a projecting condition is the existence of the plane of equal settlement. In ditch pipes the shearing forces extend all the way from the top of the pipe to the ground surface. In contrast, in a projective pipe installation if the embankment is sufficient high, the shearing forces may terminate at certain horizontal plane in the embankment known as

the plane of equal settlement. Part of the vertical pressure in the side prisms is transferred by shear to the interior prism. This transfer of pressure causes different unit strains in the interior and exterior prisms and a certain elevation above the pipe the accumulated strain in the interior prism plus the settlement of the top of the structure equal the accumulated strain in the exterior prism plus the settlement of the critical plane. Above the plane of equal settlement the interior and exterior prism of soil settle the same. In buried concrete pipe the height of the plane of equal settlement, designated as H_e, can be either real if it is less than the height H of the embankment or imaginary if it greater than H. The first case where H_e is less than H is known as the incomplete projection condition; while the second case where H_e is greater than H is known as the complete projection condition.

In calculating the vertical load on top of the concrete pipe induced by the embankment in a positive projecting condition, Equation 5 can be used.

$$W_c = C_c g B_c^{\,2} \tag{5}$$

where B_c is the horizontal breath (outside) of pipe, in meters (ft) and C_c is equal to the load coefficient for projecting condition. For the complete projection condition C_c can be calculated by Equation 6.

$$C_c = \frac{e^{2Km(H/B_c)} - 1}{2Km} \tag{6}$$

In which μ the coefficient of internal friction of fill material, H is the height of fill above the pipe in meters (ft). Also, for the incomplete projection condition, C_c can be calculated by Equation 7.

$$C_c = \frac{e^{2Km(H_e/B_c)} - 1}{2Km} + (\frac{H}{B_c} - \frac{H_e}{B_c})e^{2Km(H_e/B_c)} \tag{7}$$

where *He* is the height of plane of equal settlement, in meters (ft), which can be calculated equating an expression for the sum of the total strain in the interior prism plus the settlement of the top of the pipe to a similar expression for the sum of the total strain in a exterior prism plus the settlement of the critical plane. He can be calculated using Equation 8.

$$\left[\frac{1}{2Km} + \left(\frac{H}{B_c} - \frac{H_c}{B_c}\right) + \frac{r_{sd}\,p}{3}\right]\frac{e^{2km(H_e/B_c)} - 1}{2Km} + \frac{1}{2}\left(\frac{H_e}{B_c}\right)^2 + \frac{r_{sd}\,p}{3}\left(\frac{H}{B_c} - \frac{H_e}{B_c}\right)e^{2Km(H_e/B_c)}$$
$$-\frac{1}{2Km}\cdot\frac{H_e}{B_c} - \frac{H}{B_c}\cdot\frac{H_e}{B_c} = +\,r_{sd}\,p\frac{H}{B_c} \tag{8}$$

where r_{sd} is the settlement ratio and p the projection ratio.

Since it is both difficult and time-consuming to calculate the load coefficient for projecting pipes as seen in Equations 7 and 8, values of *Cc* can be obtained from the equations contained in Table 3. These equations are the representation of ray lines (straight lines) that relate the value of the load coefficient, *Cc*, versus *H/Bc* and have been plotted in a simply diagram as function of the ratio of the height of fill to the width of the pipe, *H/Bc*, the product of the settlement ratio and the projection ratio, pr_{sd}, and the internal friction angle of the soil, m.

Nevertheless, Marston demonstrated that the coefficient of internal friction μ has minimum effect in the calculation of *Cc* and it is unnecessary to differentiate it for different soils. Therefore; in constructing the mentioned ray lines in the diagram a customary value for $K\mu=0.19$ for the projection condition is used, in which the shearing forces are directed downward.

Table 3 Values of C_c in terms of H/B_c

rsd	Equation
+0.1	$Cc = 1.23H/Bc - 0.02$
+0.3	$Cc = 1.39H/Bc - 0.05$
+0.5	$Cc = 1.50H/Bc - 0.07$
+0.7	$Cc = 1.59H/Bc - 0.09$
+1.0	$Cc = 1.69H/Bc - 0.12$
+2.0	$Cc = 1.93H/Bc - 0.17$

Source: Soil Engineering. Spangler & Handy, 1982

Negative Projective Pipes

In this case the pipe is installed in a relative narrow and shallow trench with its top below the natural ground surface and which is then covered by an embankment as shown in Figure 3 (d). The Marston's formula for the load on a negative projecting pipe is illustrated in Equation 9.

$$W_c = C_n g B_d \tag{9}$$

where B_d represents the width of the shallow ditch in which the pipes is installed and C_n is the load coefficient for negative projecting condition.

As in the positive projecting condition, C_n can be obtained from equations contained in Tables 4, 5 y 6. These equations represent ray lines plotted in diagrams that relate the value of C_n to the ratio of height of fill to the width of the ditch, H/B_d, the settlement ratio, r_{sd}, and the coefficient of internal friction m for different values of projection ratio, p'. As in the positive projecting condition, the influence of the coefficient of internal friction m in the negative projecting condition is minimal; therefore a value of $Km = 0.13$ is commonly used for different types of soil for the negative projecting condition, in which the shearing forces are directed upward. The settlement ratio is always a negative value in the negative projecting condition lying in between -0.3 and -0.5 for the purpose of estimating loads. The projection ratio p' in the negative projection condition is equal to the depth of the ditch divided by its width.

Table 4 Values of C_n in Terms of H/Bc for $p' = 0.5$

r_{sd}	Equation
0	$C_n = 0.88H/B_c + 0.03$
-0.1	$C_n = 0.88H/B_c + 0.03$
-0.3	$C_n = 0.88H/B_c + 0.03$
-0.5	$C_n = 0.88H/B_c + 0.03$
-1.0	$C_n = 0.88H/B_c + 0.03$
-2.0	$C_n = 0.88H/B_c + 0.03$

Source: Soil Engineering. Spangler & Handy, 1982

Table 5 Values of C_n in Terms of H/Bc for $p' = 1.00$

r_{sd}	Equation
0	$C_n = 0.77H/B_c + 0.11$
-0.1	$C_n = 0.65H/B_c + 0.25$
-0.3	$C_n = 0.58H/B_c + 0.34$
-0.5	$C_n = 0.53H/B_c + 0.41$
-1.0	$C_n = 0.47H/B_c + 0.52$
-2.0	$C_n = 0.40H/B_c + 0.69$

Source: Soil Engineering. Spangler & Handy, 1982

Table 6 Values of C_n in Terms of H/Bc for $p' = 1.50$

r_{sd}	Equation
0	$C_n = 0.68H/B_c + 0.23$
-0.1	$C_n = 0.55H/B_c + 0.44$
-0.3	$C_n = 0.48H/B_c + 0.58$
-0.5	$C_n = 0.44H/B_c + 0.66$
-1.0	$C_n = 0.38H/B_c + 0.81$
-2.0	$C_n = 0.31H/B_c + 1.15$

Source: Soil Engineering. Spangler & Handy, 1982

Determination of Traffic Load

The American Concrete Pipe Association (ACPA) assumes that intermediate and thin thicknesses of asphalt or flexible pavements do not reduce the pressure induced by a wheel to the pavement subgrade any significant degree (Concrete Pipe Design Manual, 2000). Therefore, these pavements should be considered as unsurfaced roadways. A general approach in determining the resultant of live loads on buried concrete pipes establishes that the magnitude of the load on any plane in the soil will be larger at the vertical axis directly below the point of application and it will tend to decrease in all directions outward from the center of application. Moreover, as the distance between the plane and the surface increases, the intensity of the load at any point on the plane decreases. Figure 4 shows a schematic distribution of a live load in a buried pipe.

In calculating the live loads on buried concrete pipes, ACPA analyzes the live load pressure transmitted trough unsurfaced roadways to concrete pipes in accordance with the criteria of the AASHTO Load Resistance Factor Design (LRFD) Bridge Design Specification (Concrete Pipe Design Manual, 2000). The AASHTO LRFD design loads are the HS 20 with a 32,000 pound axle load in the normal truck configuration, and a 25,000 pound axle load in the alternate load configuration as shown in Figure 5. The 32,000 pound axle load and the 25,000 pounds in the case of the alternate truck design axle are carried on dual wheels as shown in Figure 6

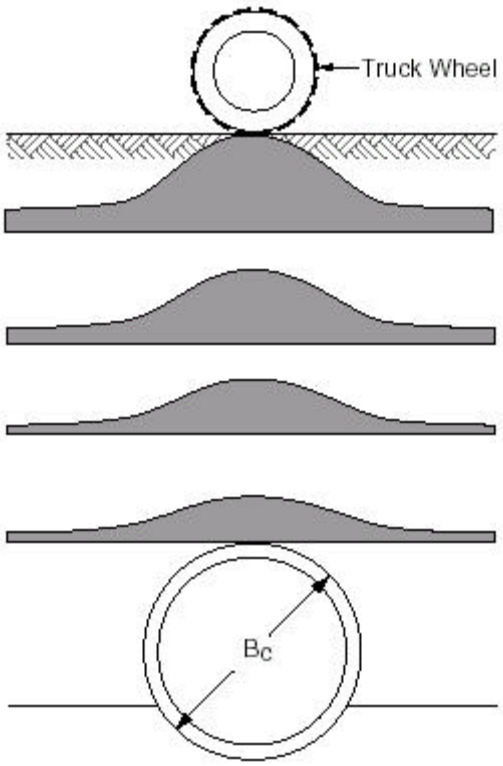

Figure 4: Live Load Distribution

Source: Concrete Pipe Design Manual 2000. American Concrete Pipe Association

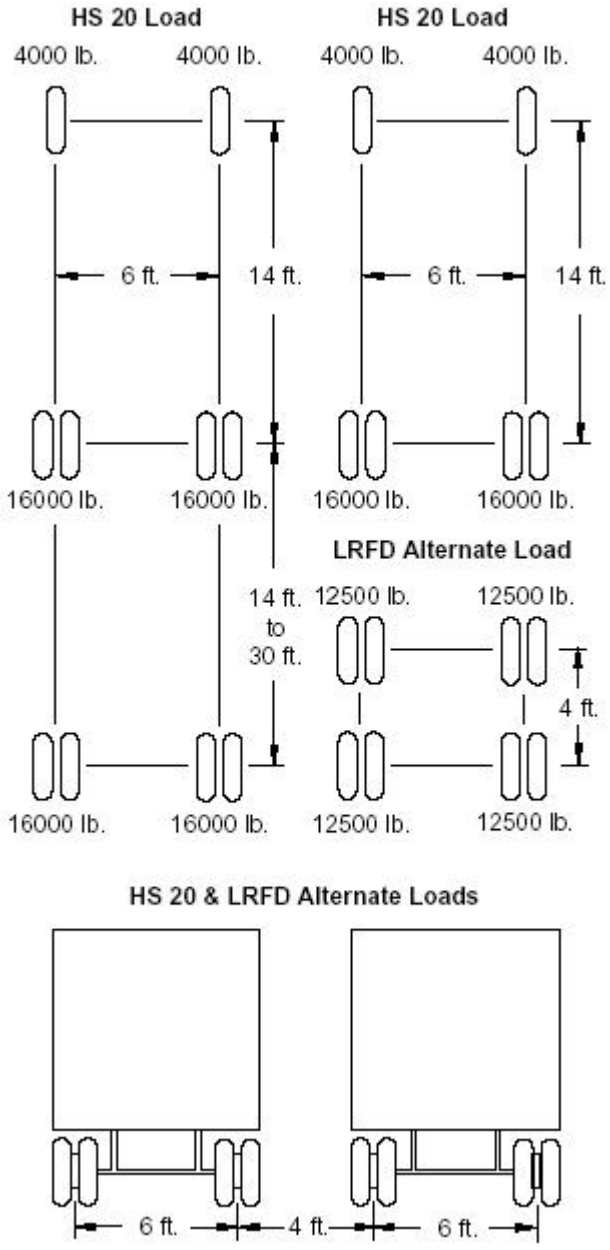

Figure 5: AASHTO Wheel Loads and Wheel Spacing

Source: Concrete Pipe Design Manual 2000. American Concrete Pipe Association

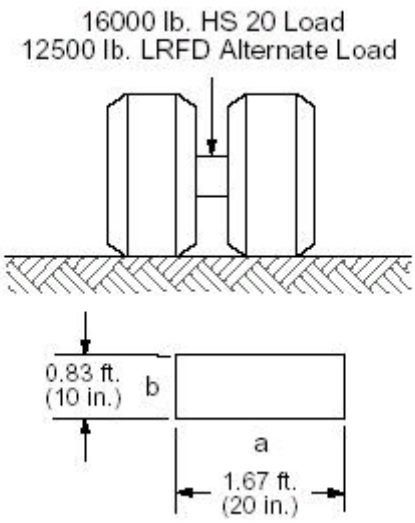

Figure 6: AASHTO wheel load surface contact area

Source: Concrete Pipe Design Manual 2000. American Concrete Pipe Association

Impact Factors

The AASTHO LRFD considers a dynamic load allowance to account for the truck load being nonstatic. The dynamic load allowance, IM, can be computed using Equation 10.

$$IM = \frac{33(1.0 - 0.125H)}{100} \tag{10}$$

where H is the height of earth cover over the top of the pipe in feet.

Load Distribution

The surface load is considered to be uniformly spread on any horizontal subsoil plane. This spread load area is the result of increasing the length and width of the surface (wheel) contact area according to different load configurations as shown in Figure 7 for a dual wheel; in

Figure 8 for dual wheels of two trucks in passing mode; and Figure 9 for two dual wheels of two alternate load configurations in passing mode.

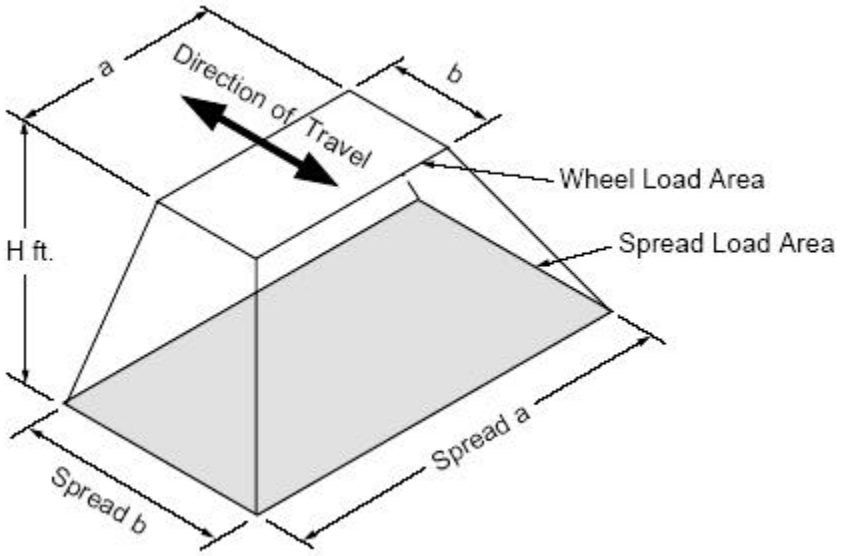

Figure 7: Spread load area for a single-dual wheel
Source: Concrete Pipe Design Manual 2000. American Concrete Pipe Association

The increase in length and width of the surface wheel load on any horizontal subsoil plane is governed by the height of earth cover over the top of the pipe as shown in Table 7.

Table 7 LRFD Wheel Contact Area Dimensional Increase Factor

Soil Type	Dimensional Increase Factor
LRFD select granular	1.15H
LRFD any other soil	1.00H

Source: Concrete Pipe Design Manual 2000. American Concrete Pipe Association

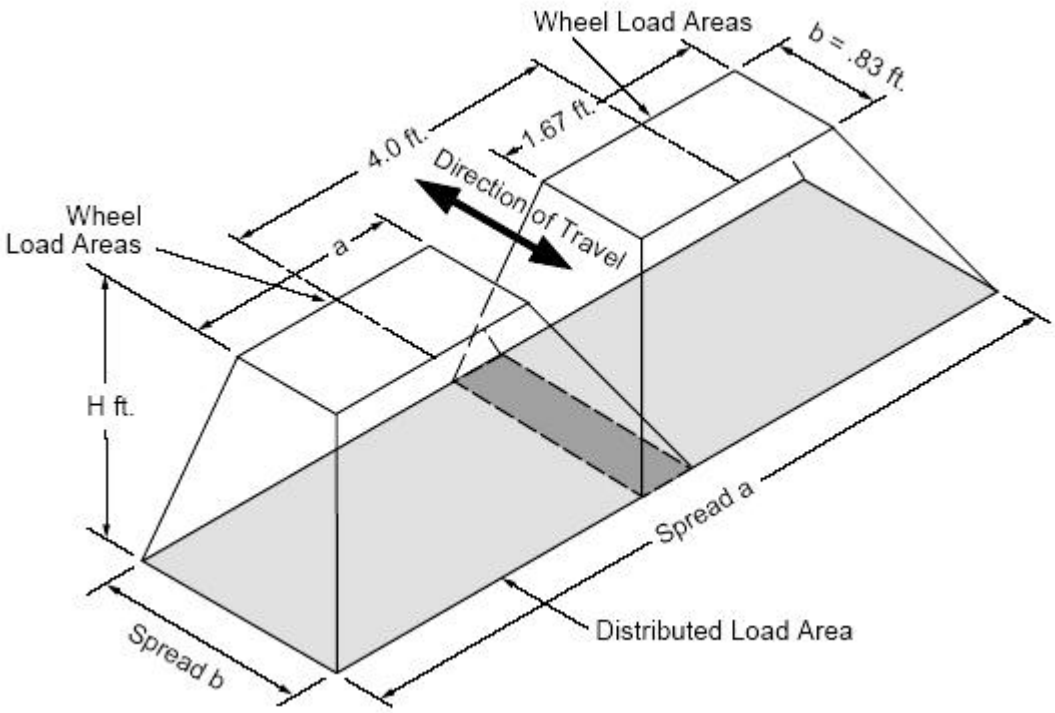

Figure 8: Spread load area for two single dual wheels in passing mode
Source: Concrete Pipe Design Manual 2000. American Concrete Pipe Association

As seen in Figures 7, 8, and 9, spread load areas from adjacent wheels overlap as the height of earth cover over the top of the pipe increases. Nevertheless, for shallow depths the maximum pressure is developed by a HS 20, 16,000-pound dual wheel, since spread load areas from adjacent dual wheels from trucks in a passing mode do not overlap at shallow depths. At intermediate depths, the maximum pressure is induced by the wheels of two HS 20 trucks in the passing mode since their spread load areas overlap and the two dual wheels apply a greater load than the 12,500 pounds of an alternate load wheel configuration. At greater depths, the maximum pressure is developed by wheels of two alternate load configuration trucks in the passing mode, since at 12,500 pounds each the four wheels apply a load of 50,000 pounds.

Establishing the exact geometric relationship of individual and combinations of surface wheel loads is an impractical task. Therefore, the most critical loading configurations along with axle loads and dimensions of the rectangular spread load area shown in Table 8 and 9 for the two AASHTO LRFD soil types.

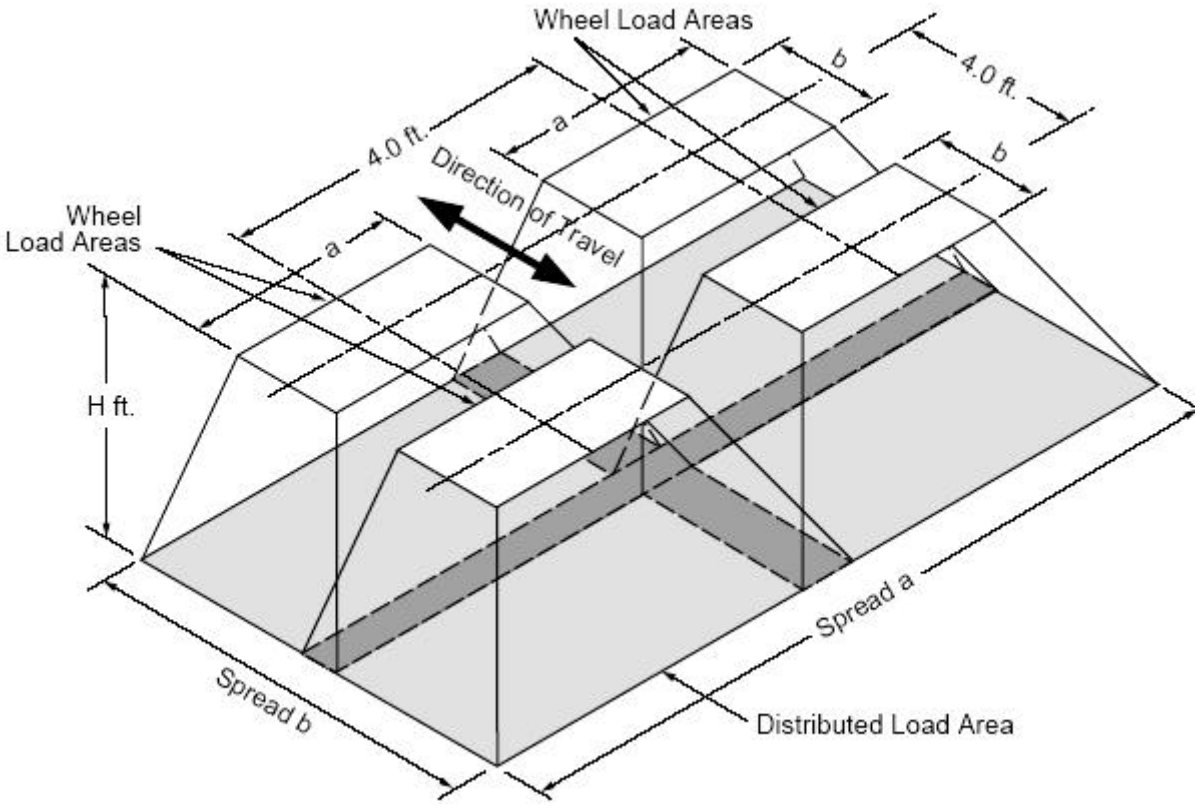

Figure 9: Spread load for a two single dual wheel of two alternate loads in passing mode
Source: Concrete Pipe Design Manual 2000. American Concrete Pipe Association

Table 8 LRFD Critical Wheel Loads and Spread Dimensions at the Top of the Pipe for Select Granular Soil Fill

H (feet)	P (pounds)	Spread a (feet)	Spread b (feet)	Figure
H < 2.03	16,000	a + 1.15H	b + 1.15H	7
2.03 = H= 2.76	32,000	a + 4 + 1.15H	b + 1.15H	8
2.76 = H	50,000	a + 4 + 1.15H	b + 4 + 1.15H	9

Source: Concrete Pipe Design Manual 2000. American Concrete Pipe Association

Table 9 LRFD Critical Wheel Loads and Spread Dimensions at the Top of the Pipe for Other Soils

H (feet)	P (pounds)	Spread a (feet)	Spread b (feet)	Figure
H < 2.33	16,000	a + 1.00H	b + 1.00H	7
2.33 = H= 3.17	32,000	a + 4 + 1.00H	b + 1.00H	8
3.17 = H	50,000	a + 4 + 1.00H	b + 4 + 1.00H	9

Source: Concrete Pipe Design Manual 2000. American Concrete Pipe Association

Average Pressure Intensity

The wheel load average pressure intensity on the subsoil plane immediately on top of the pipe can be calculated according Equation 11.

$$w = \frac{P(1+IM)}{A} \tag{11}$$

where *w* is the load average pressure intensity (pounds per square foot), *P* is the total live wheel load applied at the surface (pounds), *IM* is the dynamic load allowance, and A is the spread wheel load area at the outside top of the pipe (square feet).

Total Live Load

Moreover, AASHTO LRFD requires the application of a 640 pound per linear foot lane load applied across a 10 foot wide lane at all depths of earth cover over the top of the pipe up to a depth of 8 feet. Therefore, the total live load applied on the pipe can be calculated using Equation 12

.

$$W_T = (w + L_L)LS_L \tag{12}$$

where W_T is the total live load in pound, *w* is the wheel load average pressure intensity calculated from equation 10 in pounds per square foot at top of the pipe, L_L is the lane load as required by AASHTO in pounds per square foot, *L* dimension of A parallel to the longitudinal axis of pipe in feet, and S_L is the outside horizontal span of pipe, B_c, or dimension of A transverse to the longitudinal axis of pipe, whichever is less in feet.

The total live load in pounds per linear foot, W_L, is calculated by dividing the total live load, W_T, by the effective supporting length, L_e of the pipe as shown in Figure 10.

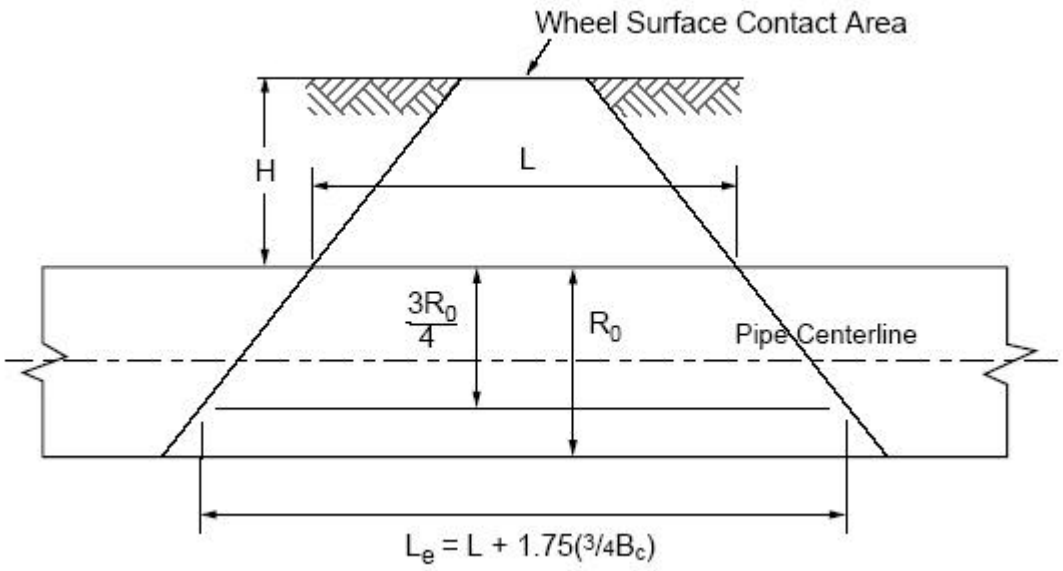

Figure 10: Effective Supporting Length of Pipe
Source: Concrete Pipe Design Manual 2000. American Concrete Pipe Association

Actual Load on Sewer Concrete Pipe underneath the Surveyed Area

To achieve one of the two main objectives of this study related to the detection of leakages in buried pipelines using GPR, a concrete sewer pipe installed under a flexible pavement was selected. The concrete pipe with an internal diameter of seven feet and a wall thickness of eight inches has an earth cover of approximately twenty one feet of sandy soil backfill. The maximum load on the mentioned pipe has been calculated in accordance with the preceding concept exposed throughout this chapter. Because of the depth of the pipe, the load on the pipe imposed by the traffic is practically negligible. The maximum live load detected at the horizontal plane on top of the pipe is approximately 160 lbs per linear foot of pipe. Nevertheless, the earth load imposed by the weight of the soil column above the pipe was significantly larger

due to the considerable diameter of the pipe. The magnitude of the load imposed by the soil immediately above the pipe (overburden) assuming a ditch condition is 19,000 lbs per linear foot. These two values represent a good approximation of the actual load condition on the mentioned sewer concrete pipe.

CHAPTER 4

EXPERIMENTAL WORK

Ground Penetrating Radar Survey

An extensive leak detection survey was carried out using ground penetrating radar (GPR) to determine the effectiveness of this technique in detecting leaks in buried concrete pipes. The GPR survey was performed on a delimited area at University Boulevard westbound near the intersection of University Boulevard and Rouse Road, as pictured in Figure 11.

Figure 11: Aerial photograph of site location in GPR survey
Source: Orange County Florida Property Appraiser

At this location, a concrete sewer pipe, seven feet in diameter, which flows wastewater to the Iron Bridge Reclamation Facility, Seminole County in Florida is buried at a depth of approximately 21 feet according to the facility staff. The selection of this site is because of the evident subsidence of pavement surface over the past years due to a leakage across the buried pipe. In the past years a significant number of patches and overlays have been conducted in this area.

Instrumentation

Data acquisition was performed using the SIRveyor SIR-20 manufactured by Geophysical Survey Systems, Inc. (GSSI). This GPR system represents one of the most recent additions to GSSI's line of GPR products. The SIRveyor SIR-20 consists basically of a radar control unit and a storage/display device (laptop) named tough book that in connection with the transceiver/receiver antenna conformed the equipment used in the detection of underground leakages. The data collection unit, the laptop PC and, the 80 MHz antenna are shown in Figure 12.

The antennas used during the survey were of the unshielded type with centre frequencies of 300 and 80 MHz. Raw data collected was processed using the Windows-based RADAN NT post processing data software version 5, provided by GSSI.

The data collection and processing parameters during the survey were as follow: antennas having 300 and 80 MHz center frequencies with ranges of 150 and 200 ns respectively; vertical high pass filter and vertical low pass filter equal to 25 and 200 MHz; scans per second equal to

32; transmit rate of 32 KHz; and; stacking equal to 32 scans. All subsurface profiles shown in this study has been depicted using the parameters previously mentioned.

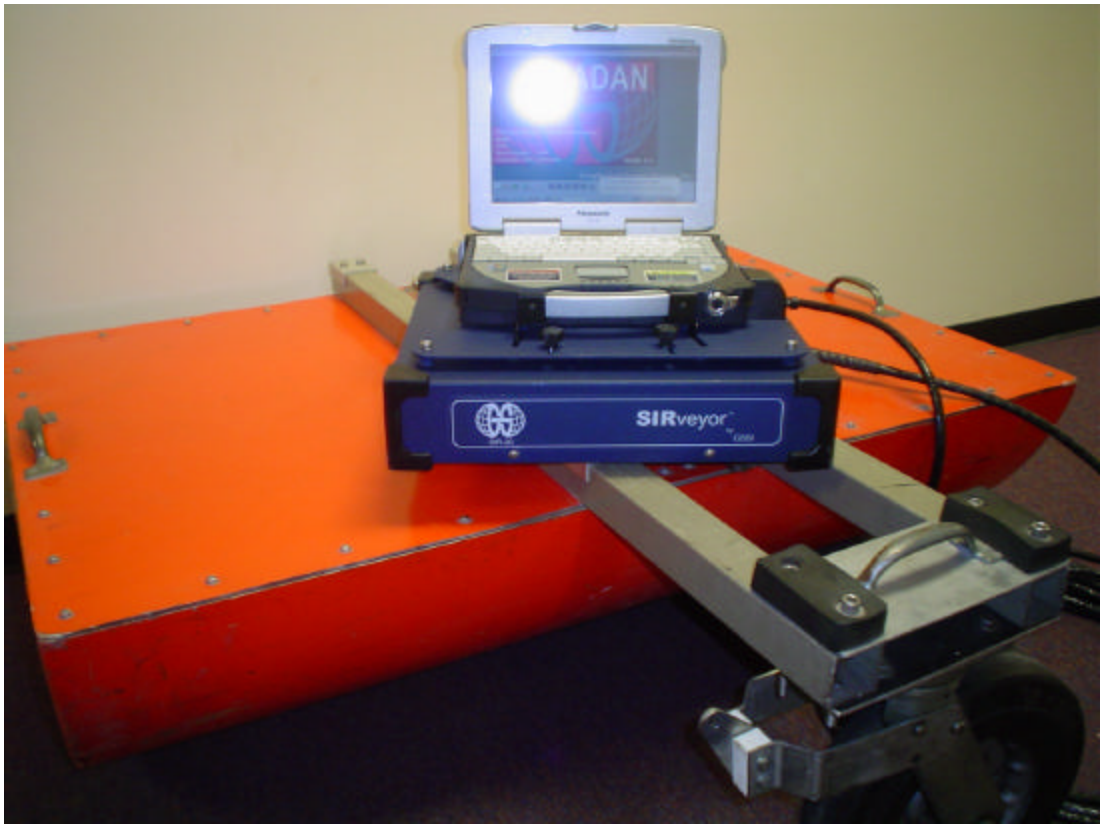

Figure 12: The SIRveyor SIR-20 and 80MHz Antenna

Description of Tests

In order to facilitate the acquisition of data, a 160 feet by 48 feet survey grid was marked over the area of study. The grid delimits an area over the suspected leakage and further away from it. The grid's main axis was determined to follow the center of the sewer pipeline. Besides, grid lines were spaced at 20 feet intervals in the north-south direction, perpendicular to the grid's

main axis. The east-west boundaries of the grid were fixed to be at 40 feet east and 90 feet west from the suspected leakage location; and the north-south boundaries were located at 18 feet north and 30 feet south from the grid's main axis as shown in figure 13.

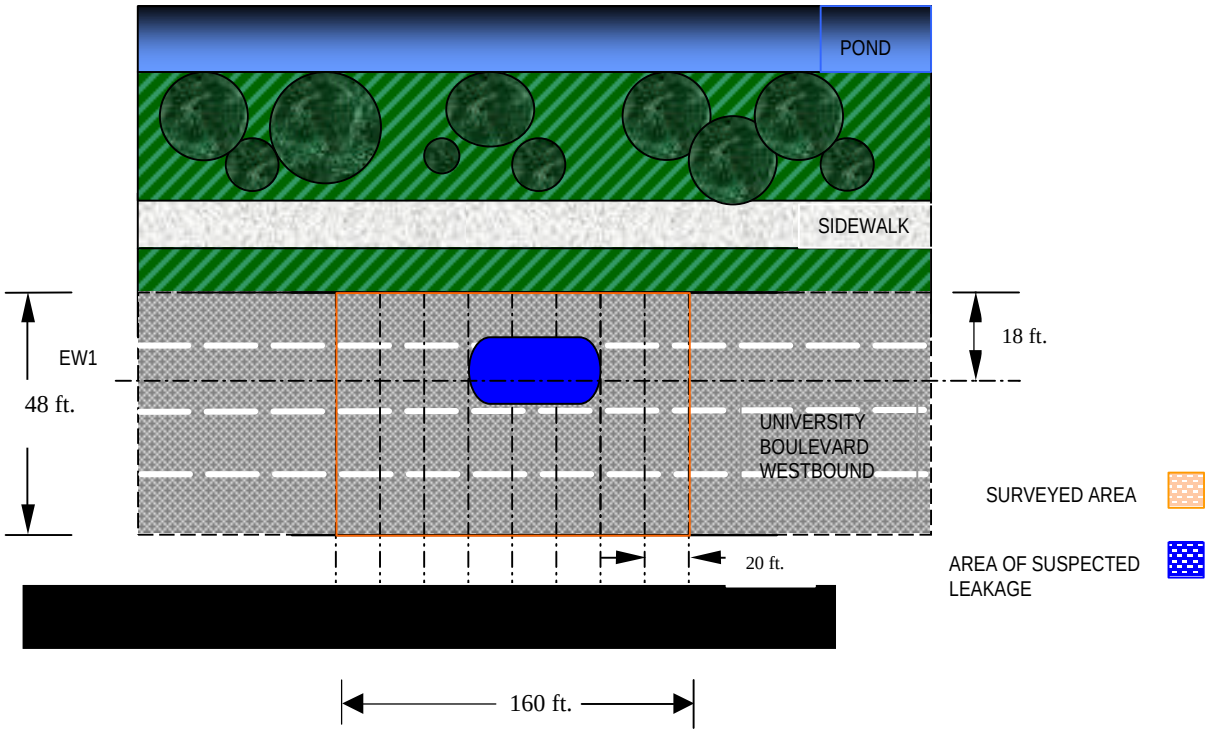

Figure 13: GPR Survey Grid

Radar data were collected along the grid's main axis parallel to the pipeline (EW1) and along the 10 grid lines perpendicular to the pipeline (NS1, NS2, NS3, NS4, NS5, NS6, NS7, NS8, and NS9)

As it has been mentioned before, the radar survey was performed using antennas having 300 and 80 MHz center frequencies. Antennas were pulled manually for survey lines

perpendicular to the pipe (from NS1 to NS9) and hauled by a vehicle during the survey line parallel to the pipe (grid's main axis, EW1).

In calibrating depth of penetration, a dielectric constant of 6 was selected during the survey. This value as recommended by the SIRveyor SIR-20 user's guide 2002 represents a good approximation of the dielectric constant for sand, primary component of the earth material at the survey area.

Fiber-Wrapping Technique for Repairing and Strengthening Pipe Joints

As mentioned under scope of research, in order to investigate the capability of the FRP wrapping technique to strengthen and repair the cracked or faulty pipe joints, laboratory tests were conducted. The experimental research consisted basically of two (2) laboratory tests performed in large-scale pipe joints wrapped with carbon fiber reinforced polymer (CFRP). A total of two concrete pipe bell-spigot joints, denoted as 3F-0/90 and 3F-45/45, were tested. In both specimens the jacket thickness used was of three plies. Nonetheless, the saturated fabric of specimen 3F-45/45 was applied in such a manner that the orientation of carbon fibers was at 45 degree angle with respect to the horizontal. Likewise, the orientation of carbon fibers for specimen 3F-0/90 was defined to be 0 and 90 degrees. Table 10 summarizes the test matrix

Table 10 Test Matrix

Specimen Designation	Jacket Thickness	Fabric Fiber Orientation
3F-0/90	3	0/90
3F-45/45	3	45/45

One of the laboratory tests consisted of the application of a force over the repaired joint to determine the structural capability of the FRP jacket to resist the applied load. The magnitude of the test force was calculated in accordance to the ASTM standard designation C 497 – 03a (Standard Test Methods for Concrete Pipe, Manhole Sections, or Tile) under section 13, which refers to Joint Shear Test. The second test consisted of capping both pipe ends and filling them with water to determine the effectiveness of the technique in stopping leaks at the repaired joint.

Materials

The main materials used in this study were circular reinforced concrete pipes with bell and spigot joints, hydro-stone® gypsum cement and fiber reinforced polymer composites. The following is a brief description of their properties.

Circular Reinforced Concrete Pipe

The reinforced sewer pipes involved in this study are in accordance, with ASTM designation: C 76-03. These pipes possess bell and spigot joints with rubber gaskets in accordance with ASTM C 361 and C 443. Materials used in the manufacture of concrete sewer pipe comply with the following ASTM specifications: Portland cement, C 150 Type II and Aggregates, C 33. Characteristics of the concrete pipes are described as follow:

- Nominal pipe internal diameter (inches): 15
- Bell overall diameter (inches): 24.40
- Wall thickness (inches): 2.25
- Pipe length (feet): 8

- Pipe Weight (pounds per foot): 140

Hydro-Stone Gypsum Cement

Hydro-Stone Gypsum cement is a high strength plaster with high water absorption resistance used in novelty castings, molds and figurines. Since the bell and spigot ends created a joint with an uneven surface that made difficult to wrap the saturated carbon fabric around the joint, a Hydro-stone Gypsum Cement rim was constructed around the joint itself creating a level surface for the wrapping of the FRP as pictured in Figure 14. Technical properties of Hydro-Stone are listed in Table 11.

Figure 14: Hydro-Stone rim around pipe joint

Table 11 Hydro-Stone™ Gypsum Cement Technical Properties

Technical Properties	ENGLISH	METRIC
Use consistency (parts of water by weight per 100 parts plaster)	32	32
1 Hr. compressive strength	4,000 psi	27.6 MN/m^2
Dry compressive strength	10,000 psi	69.0 MN/m^2
Maximum setting expansion	0.240%	0.240%
Density (wet)	119.0 lb/ft^3	1.91 g/cm^3
Density (dry)	108.0 lb/ft^3	1.73 g/cm^3
Set time (machine mix)	17-20 min.	17-20 min.

Source: Hydro-Stone™ Gypsum Cement. United States Gypsum Company, 1999

Hydro-Stone Mix Design, Casting and Cured

It was estimated that 3.60 cubic feet of Hydro-Stone mixture would be sufficient to cast the octagonal rim around the pipe joint. The two mixture components, Hydro-Stone and water, were weighed according to the use consistency of 33 parts of water by weight per 100 parts of plaster. The quantities of material per rim casting at each joint consisted of:

- Hydro-Stone Gypsum Cement: 300 lbs.
- Water: 100 lbs.

The product was mixed by a batch process. The mixing was done in 10 different portions; each of them in a 5 gallon bucket with 30 lbs of Hydro-Stone and 10 lbs of water as shown in Figure 15.

Figure 15: Mixing of the Hydro-Stone in a batch process

The Hydro-stone was strewed into the water slowly and evenly allowing soaking for 3 minutes. Subsequently, the two components, gypsum cement and water, were mixed during approximately 4 minutes using a hand-held electric drill with a blade propeller. Once elapsed the mixing time the mixture was poured into an octagonal wooden formwork previously oiled to prevent the adherence of the Hydro-Stone to the mold walls. In pouring the different portions of mixture, a time of 4 minutes elapsed in between consecutive portions. The formwork was constructed in a way that it could be split lengthwise to facilitate its removal once the Hydro-stone hardened, as shown in Figure 16. A total of three people were necessary to complete the

mixing process. During the casting process the formwork was gently knocked to prevent trapped air at or near the surface of the cast piece. The timber mold was removed about 2 hours after the mixture casting was completed.

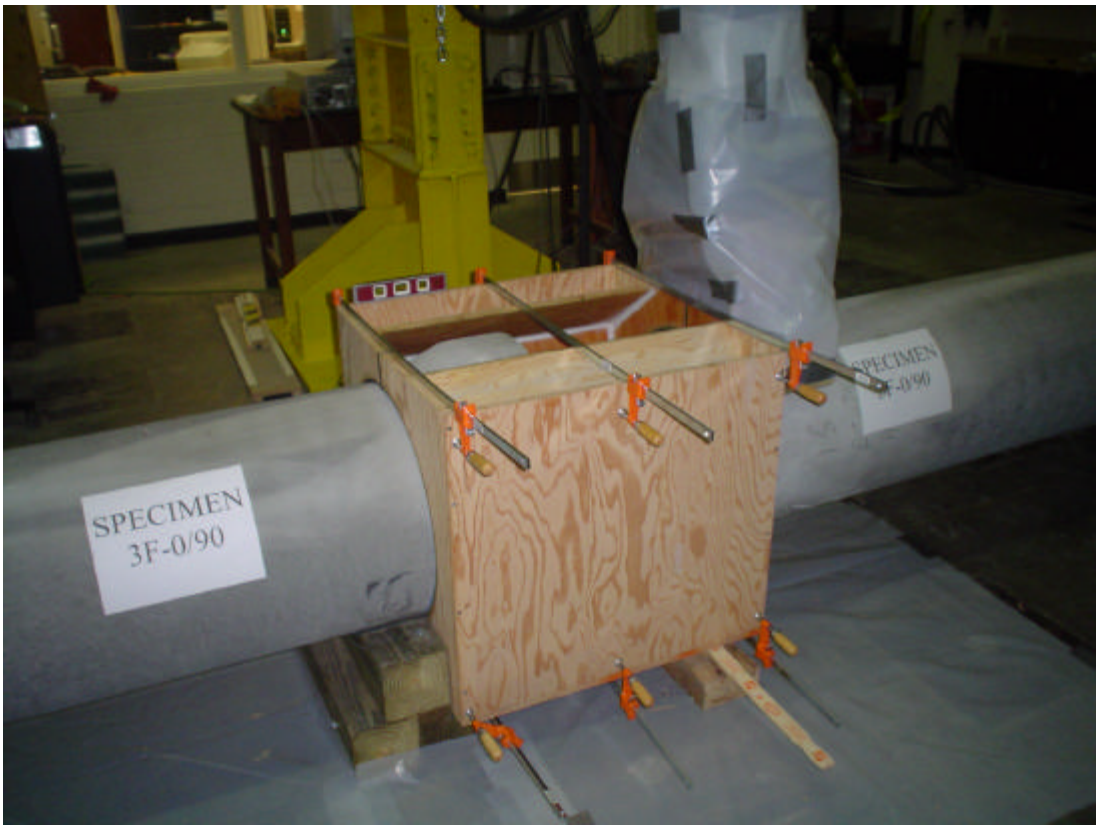

Figure 16: Wooden formwork placed around the joint

Fiber Reinforced Polymer Material (FRP)

The composite material used in this study was created by saturating a carbon fiber sheet with a epoxy resin. The carbon fabric and saturating epoxy resin referred herein as QuakeWrap^{TM} and QuakeBond^{TM} J300-SR respectively are trademark materials of QuakeWrap

Inc, in Tucson, AZ. Both materials are pictured in Figure 17. It is important to mention that the author of this study does not endorse the use of QuakeWrap™ and QuakeBond™ J300-SR; the mentioned materials have been just used for practical purposes in the development of this investigation. Properties of QuakeWrap™ and QuakeBond™ J300-SR are summarized in Tables 12 and 13 respectively.

Figure 17: QuakeWrap™ and QuakeBond™ J300-SR

Preparation and Installation of FRP

The carbon fabric was cut in straps of 27 inches wide by 8 feet long for the specimen 1 in which the FRP straps would be applied in such a way that the carbon fibers would describe an

orientation of 0 and 90 degrees with respect to the longitudinal axis of the Hydro-Stone rim. On the other hand, in preparation of specimen 2 the carbon fabric was cut in strips of 27 inches wide by a maximum of 4 feet long because of the dimension of the fabric roll. For specimen 2 the carbon fabric was cut making the carbon fibers describe an orientation of + 45 / -45 degrees with respect to the longitudinal axis of the Hydro-Stone rim when wrapped around the joint.

Table 12 QuakeWrap™ Specifications[1]

Product Designation	TB20C
Packaging	Roll of Fabric: 50 inch wide x 200 foot long
Description	Fabric
Fiber Orientation	0/90
Fiber Type	Carbon
Effective Thickness per Ply (inches)	0.05
Density; ASTM-D792 (g/cm^3)	1.27
Direction Tested (Long. or Trans.)	L & T
Maximum Load Per Inch Width (lb)[2]	2,250
Tensile Strength; ASTM-D3039 (ksi)	45.1
Modulus of Elasticity; ASTM-D3039 (ksi)	6,440
Elongation at Failure (%)	-

[1] The above results were obtained based on samples produced with two plies of fabric and under ideal laboratory conditions from a single lot. The average resin content of samples measured in accordance with ASTM-D2584 is in between 55% to 60% by weight. Due to variation in material properties from different lots, a strength reduction factor of 20% must be applied to the above values.
[2] Values are reported for a single ply of fabric

Source: Quakewrap, Inc. Tucson, AZ.

Table 13 QuakeBond™ J300-SR Specifications

Weight per gallon	Part "A" 9.4 lbs, part "B" 8.3 lbs
Mix ratio	2:1 by volume (100:45 by weight)
Viscosity mixed	Medium, Thixotropic
Pot life at 77° F	60 minutes
Compressive strength, ASTM D695	> 10,000 psi
Tensile strength, ASTM D638	9,500 psi
Tensile elongation, ASTM D638	8.0 %
Bond strength to concrete (Elcometer)	300 psi minimum, w/100% substrate failure
Water absorption (% gain) 24 hrs	<1
Thin film set time@ 77 °F	3-4 hours
Full cure time	24-48 hours

Source: Quakewrap, Inc. Tucson, AZ.

Next, two litters of resin (part A) was mixed with a litter of hardener (part B) following the mix ratio of 2:1 by volume suggested by the manufacturer. The product was mixed thoroughly in a 3-gallon bucket by hand for approximately 5 minutes. Special attention would be taken for colored lines in the mixture that represent uncombined resin and the mixing of the resin, if necessary, would continue until a uniform color was achieved. The dry fabric straps were fully

saturated on one face with the resin using a foam roller. Straps fabrics were impregnated with the resin until a wet appearance in the fabric occurred. Subsequently, the saturated carbon straps were wrapped around the hydro-stone rim surface. As the saturated fabric straps were installed, they were pressed against the surface of the hydro-stone rim helping the resin trespass the carbon fabric from underneath to the top. Moreover the FRP straps already in place were slightly coated with more resin before applying the new FRP layer. Hand pressing and a porcupine roller were used to remove any air bubbles from the fabric. A total of three plies of saturated fabric were installed on top of one another at the hydro-stone rim around the joint, and edges and overlays of the fabric straps carefully coated. Full cure time would be achieved after 48 hours (Quakewrap Inc).

QuakeBond™ J200-TC Tack Coat

In order to achieve a quick bonding between the FRP and the surface substrate (hydro-stone rim), QuakeBond™ J200-TC, a high strength structural epoxy adhesive was used. The QuakeBond is a two component material (part “A” black and part “B” white) with an immediate high tack consistency allowing it to hold the fabric saturated with J300-SR resin in place, particularly in overhead surfaces, such as at the bottom of the hydro-stone rim around the joint where gravity pulls downward the heavy saturated carbon fabric. Properties of J200-TC are shown below in Table 14.

Table 14 QuakeBond™ J200-TC Tack Coat

Weight per gallon	Part “A” 10.2 lbs, part “B” 8.44 lbs
Mix ratio	1:1 by volume
Viscosity mixed	Non-sagging thixotropic paste
Pot life at 77° F	45 minutes
Compressive strength, ASTM D695	> 4,500 psi
Tensile strength, ASTM D638	> 5,000 psi
Tensile elongation, ASTM D638	> 10%
Water absorption (% gain) 24 hrs	< 1
Full Cure Time	12 – 24 hours

Source: Quakewrap, Inc. Tucson, AZ.

Preparation and Application of QuakeBond J200TC

It was determined that 1 litter of QuakeBond J200TC would be sufficient to cover the surface of the lower part of the hydro-stone rim around the joint for each specimen. Therefore, a half litter of QuakeBond part “A” and a half litter of part “B” were mixed to comply with the mix ratio of 1:1 by volume specified by the manufacturer. Both parts, A and B, were mixed thoroughly in a 2 ½ quart bucket with a clean paint stick for approximately 5 minutes or until a consistent gray color was observed as shown in Figure 18. Even though QuakeBond J200TC bonds well with minimal surface preparation, dust and dirt were removed from the surface of the Hydro-stone rim before its application. The mixed QuakeBond J200TC was applied uniformly

over the clean surface using a putty knife until a thickness of 40 mil was achieved. The tack coat would remain workable for about 2 hours (Quakewrap Inc.)

Figure 18: Mixing of QuakeBond J200TC

Insulating Foam Sealant and Silicone

Insulating foam sealant was used to fill the gap created by the absence of the rubber gasket and disjointing of the pipes. The foam expands filling the void forming a permanent, airtight and waterproof bond to concrete. The foam sealant used was tack free in 10 minutes and cured in 8 hours. Also, a elastomeric latex sealant was used to improve the sealing condition of the foam sealant and fill small gaps in order to maintain the watertight condition of the repaired joint.

Test Preparation

The general procedure to accomplish the test program of this study involved seven (07) steps. Each step is described in detail as follow.

1. Two pipes were assembled and placed under the portal load frame as pictured in Figure 19. The pipes were supported by timber cradle blocks, which had one face curved to match the outer diameter of the pipe barrel. The rubber gasket in the joint was intentionally withdrawn and the spigot end inside the bell was pulled back one and a half inch approximately from its standard position in order to simulate a faulty joint. Figure 20 shows the disjointing in between the bell and spigot ends.

Figure 19: Testing Setup

Figure 20: Displacement of the spigot from its regular position

2. Expansible foam sealant was used to fill the space in between the bell and spigot surfaces caused by the absence of the rubber gasket. Later, the free outer surface of the expandable foam was trimmed and coated with silicone providing a watertight condition to the joint as pictured in Figure 21. During the sealing process there was a short length at the lower part of the joint circumference that could not be filled with

the expansible foam since the opening was not sufficiently large to let the foam enter. Nevertheless, silicone was used in this zone to maintain the watertight condition.

3. The octagonal formwork was placed around the joint and the Hydro-stone poured into the mold as shown in Figure 22. Dimensions of the formwork are shown in Figure 23. The design, mixing and cured of Hydro-stone were carried out as previously described at the beginning of this chapter in “Hydro-stone Mix Design, Casting and Cured”. Two hours later the formwork was removed and the hydro-stone casting provided a uniform surface to wrap the FRP around the joint as referred in Figure 24.

Figure 21: Sealing of the pipe joint

4. The two-component tack coat QuakeBond J200TC was prepared following the procedure already described under “Preparation and Application of QuakeBond J200TC” in the previous section. A layer having a thickness of 40 mil was applied over the Hydro-stone surface at the lower part of the joint to keep the saturated fabric in place.

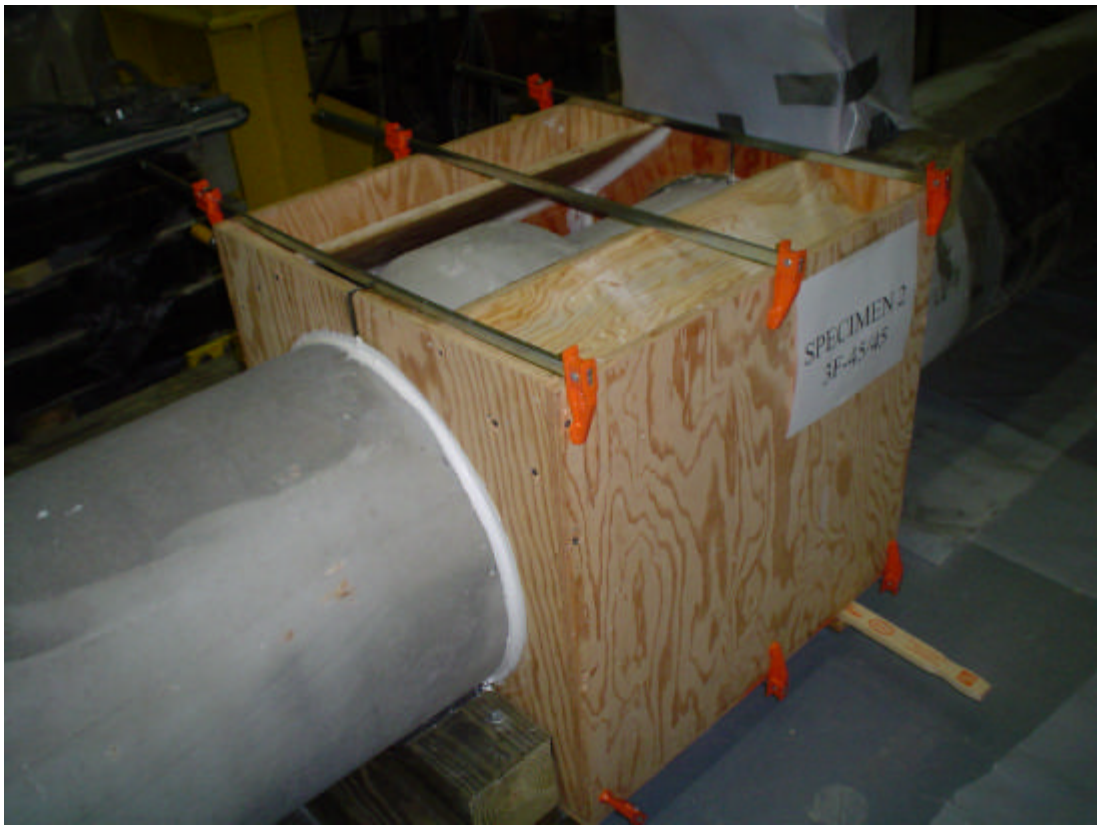

Figure 22: Installation of formwork for Hydro-Stone casting

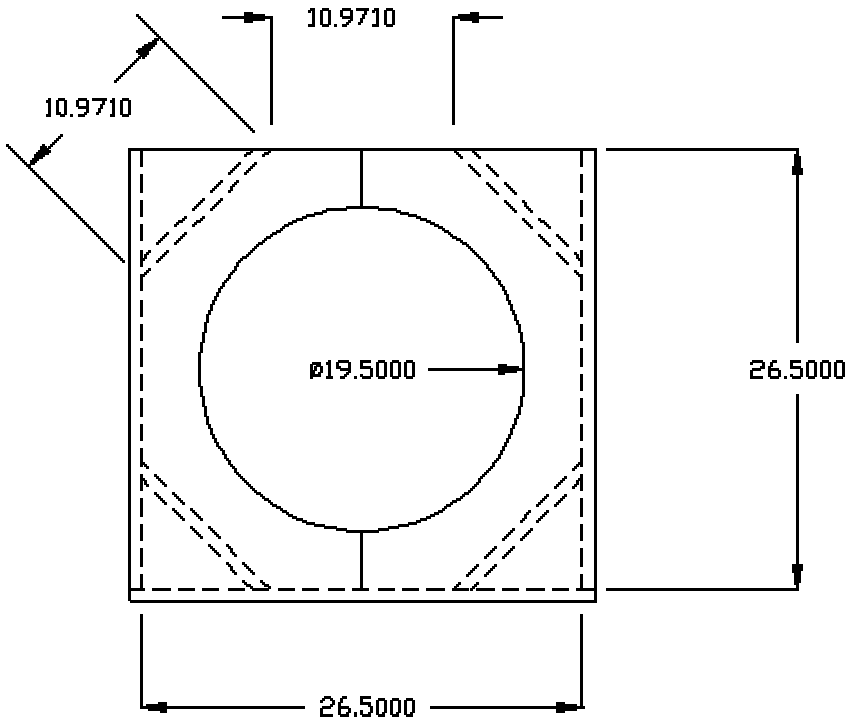
10.9710
10.9710
ø19.5000
26.5000
26.5000

(a)

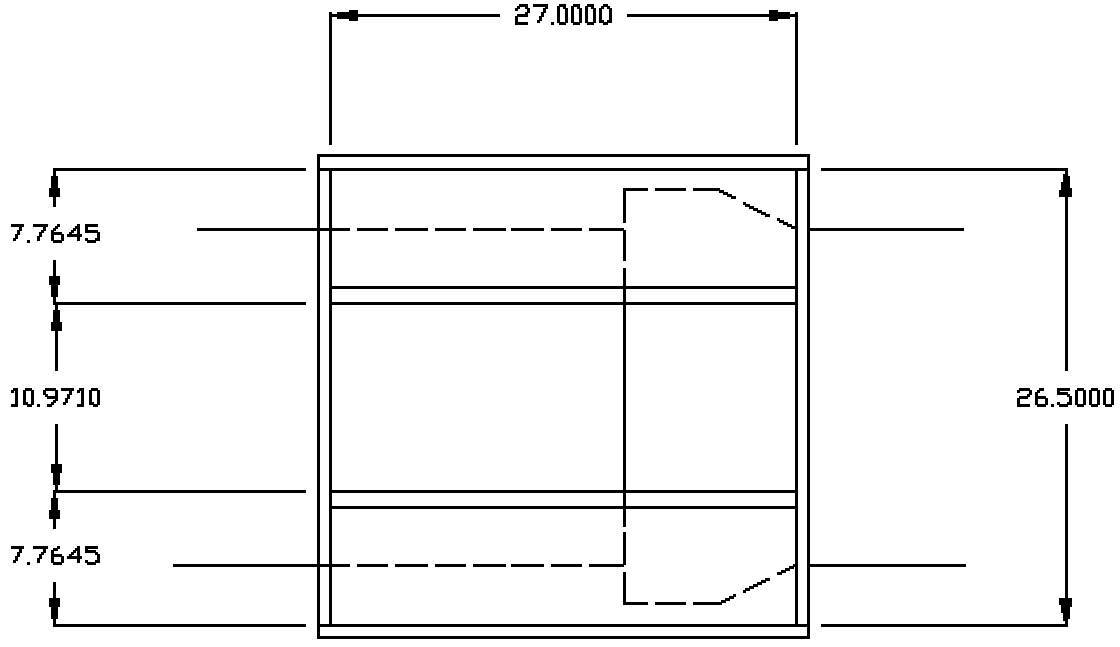
27.0000
7.7645
10.9710
7.7645
26.5000

(b)

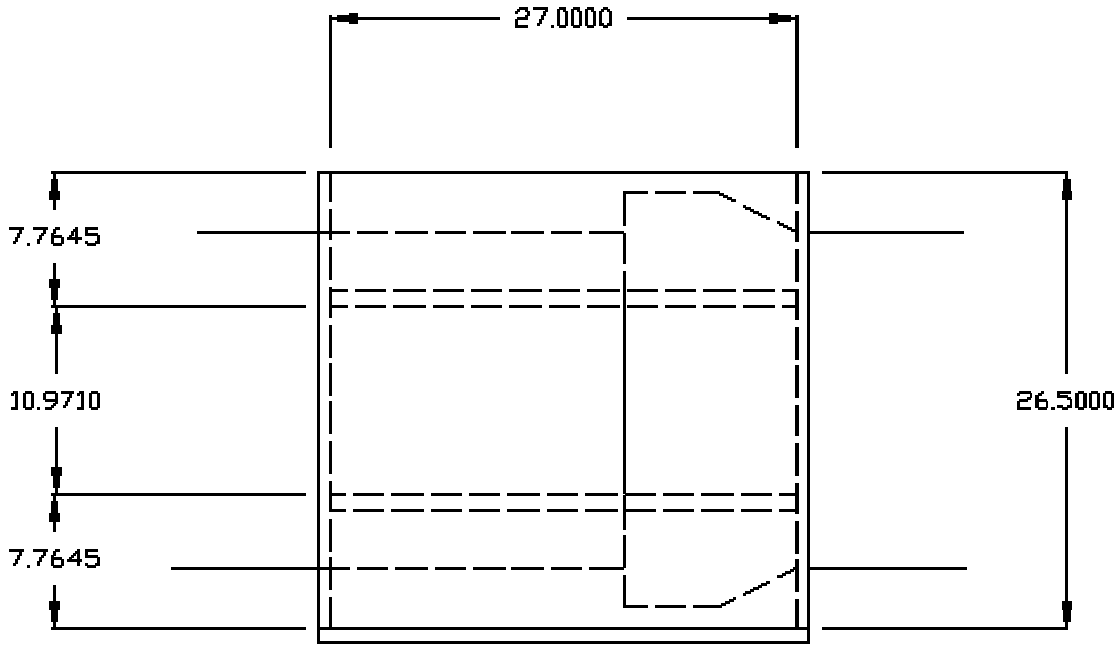

(c)

Figure 23: Formwork Dimensions. (a) Front View. (b) Top View. (c) Lateral View

5. The FRP straps were wrapped around the hydro-stone rim immediately after the application of the tack coat QuakeBond J200TC achieving a thickness of three plies as pictured in Figure 25. Preparation and application of FRP was performed as explained previously in this chapter under section “Preparation and Installation of FRP”. As recommended by the manufacturer, the time for total cured of the FRP was set in 48 hours. After wrapping the joint with FRP in specimen 3F-0/90, the carbon fibers described orientations of 0 and 90 degrees with respect to the longitudinal axis of the pipeline while specimen 3F-45/45 described orientations of -45 and +45 degrees.

Figure 24: Hydro-stone rim around the joint

6. Followed, strain gauge rosettes were attached to each specimen as described further under “Test Instrumentation”.
7. Both free ends of the pipes were capped using wooden lids to further fill them up with water as part of the experimental tests to which the specimens were subjected. Figure 26 illustrates one of the pipe ends capped with the wooden lid.

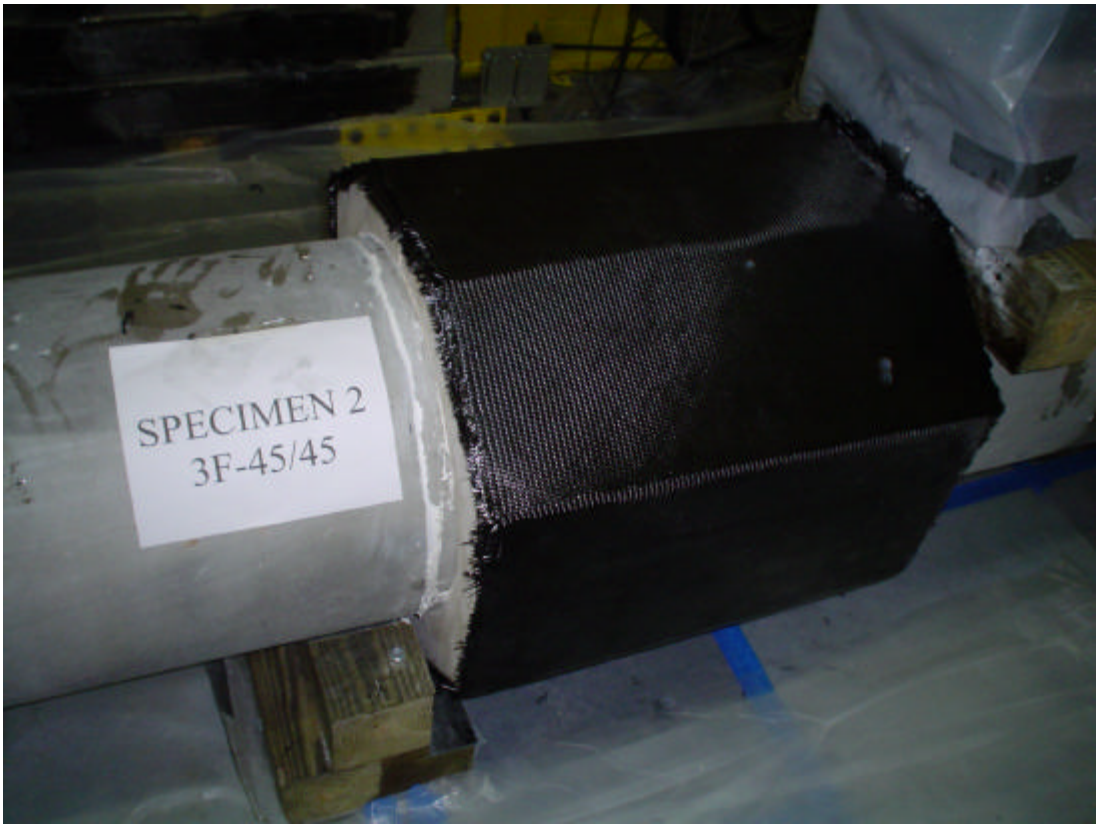

Figure 25: FRP straps wrapped around the restored joint

Test Instrumentation

In order to monitor and measure extensional strains at different points in each specimen during loading, rectangular strain rosettes were attached to the surface of the FRP jacket around the joint. Some of the strain rosettes were constructed clustering together three individual electric strain gauges at a point following three different directions, 0, 45, and 90 degrees with respect to the longitudinal axle of the pipe while the remaining ones were rectangular rosettes with gauges already grouped together in one piece and spaced 45 degrees. The strain gauges were located at the sides and top of the FRP jacket. Thus, a total of 3 rectangular strain rosettes were attached to

each specimen as shown in Figure 27. The FRP surface where the gauges were placed was sanded and cleaned with acetone to remove the resin dust from the sanding. Next, the surface was treated with an acidic substance and a neutralizer to prepare the surface for a better bonding in between the FRP surface and the gauges. Then, super glue was applied to the fabric surface and the strain rosettes were pressed against the glued surface.

Figure 26: Capping of pipe ends

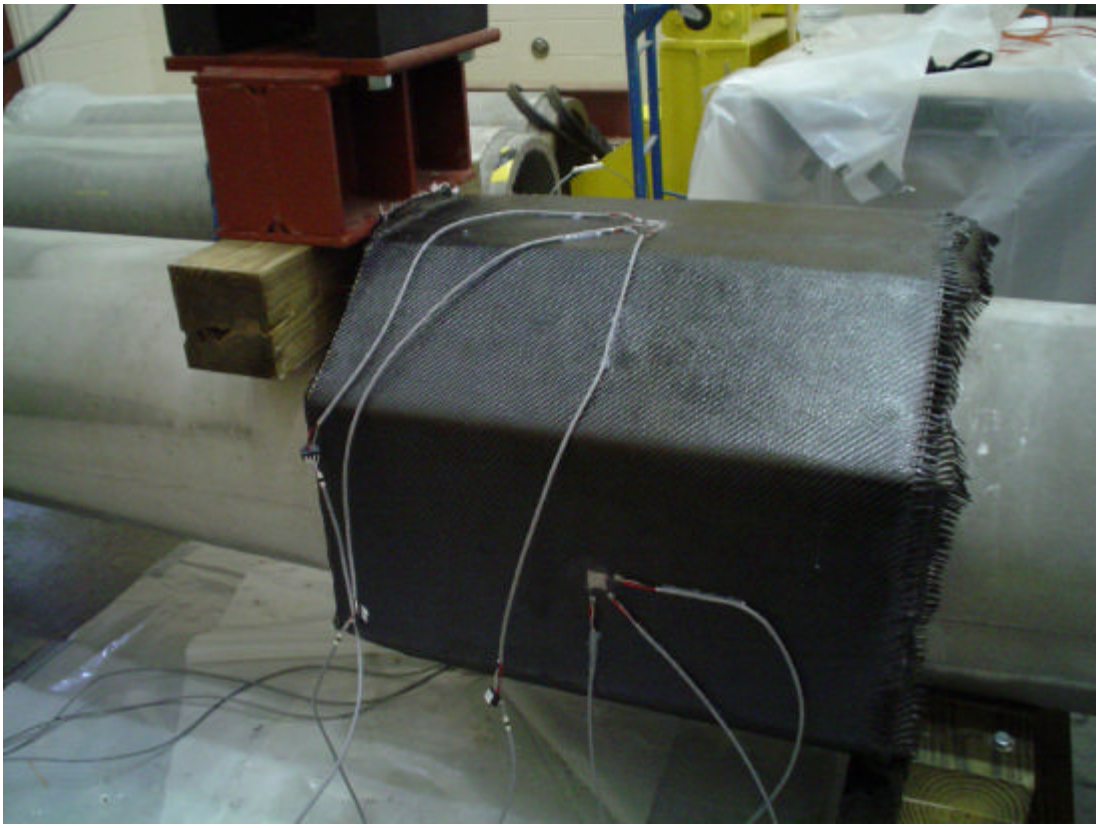

Figure 27: Strain gauge rosettes attached to the FRP jacket

Test Procedure

Laboratory testing of the specimens was carried out at the Structure's Laboratory of the University of Central Florida. The testing device was a MTS servo controlled hydraulic actuator assisted by a FlexTest II controller with a comprehensive software package that performed all test control, function generation and data acquisition. Once the specimen was placed under the portal load frame and prepared for testing as described previously under "Test Preparation", a timber cradle block with one face curved following the outer diameter of the pipe was used to distribute the load from the actuator to the pipe surface. In accordance with ASTM C497-03a, the specimens would be subjected to a vertical test load (F) applied to the suspended portion of

the test joint until the total differential load (R), including the weight of the pipe, would be 4,000 pounds per foot of pipe diameter. Figure 28 illustrates the layout of the specimen and the locations of the test force, F, and the required reaction, R; as required by the ASTM standard under section 13, which refers to joint shear test. Both parameters have been calculated and presented in Appendix A. Once the specimen was ready for testing, the actuator was initiated and the actuator's piston was watchfully pulled down until it reached the top of the timber block; at that moment the piston displacement was stopped. Subsequently, the test load (F) estimated in 5,600 lbs was applied to the unsupported spigot of the joint for one minute. The specimen was loaded to the required test force (F) at a constant rate of 0.10 inches per minute in a displacement control mode. Later, in order to determine the watertightness of the repaired joint after subjected to the test load (F), the pipes previously capped were filled with 75 gallons of water inundating only half of the pipe section as shown in Figure 29.

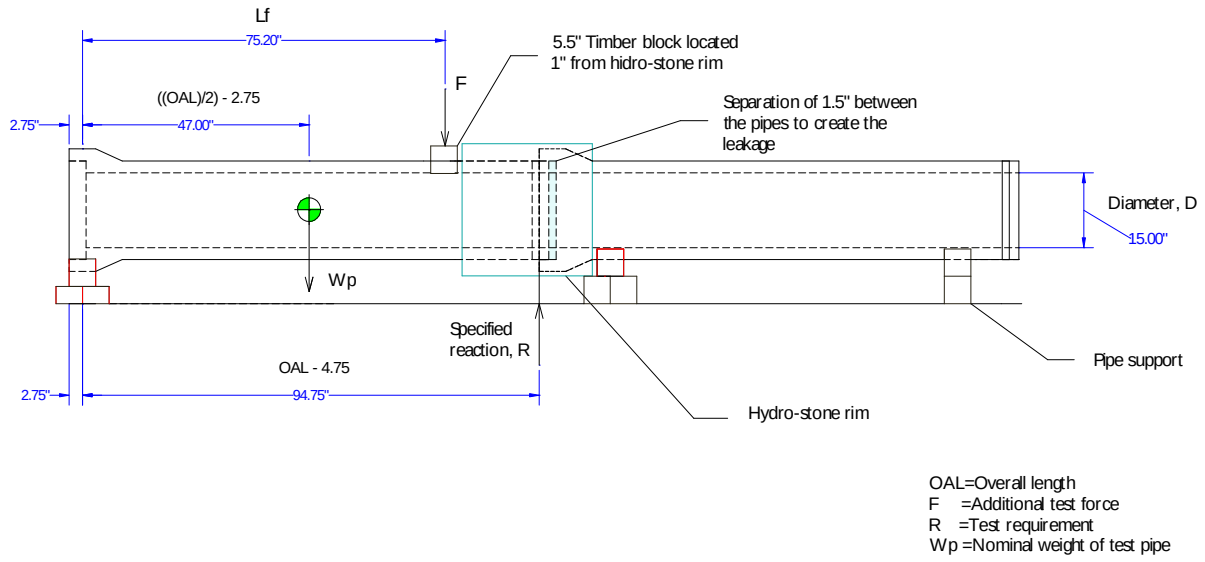

Figure 28: Setup of the Specimen and Location of Vertical Force (F) and Reaction (R)

Test Observations

The first specimen tested was the 3F-90/0. The latter was capable of resisting the shear action created across the joint as a result of the application of the test load (F) in accordance with the ASTM standard test. No visible indication of a sudden reduction of the test load (F) during the ramp up demonstrated the capacity of the joint in resisting the shear force. The strain gauges attached to the FRP surface reported very small strain values (less than 12 microstrains) characterized by a fluctuant behavior shifting back and forth uncertainly making them negligible. This strain gauges behavior led to think that the shear force imposed at the joint was entirely resisted by the spigot-bell joint and hydrostone rim. Therefore, up to this moment no additional strength, at least no determined by this test, was provided by the FRP in resisting the induced shear force across the joint.

After completed the loading test, the specimen was filled with water. A few minutes later the joint started to leak allowing water flow out through the interface in between the Hydro-stone and the pipe surface as shown in figure 30. Particular interest arose in determining whether the application of the test force (F) had weakened the sealing around the joint. Thus, the second specimen, specimen 3F-45/45, would be filled with water prior to the application of the vertical force (F).

In order to determine the ultimate strength of the joint, an additional loading test was performed, in which the same specimen 3F-0/90 was tested to failure. The location of application of the test load (F) remained the same as in the previous test; only the location of the pipe supports was modified. The support located near the joint was removed as shown in Figure 31. The assembled pipes were supported only at their ends with a spam length of 15 feet. This

scenario recreated one of the most unfavorable bedding conditions in the field where the subsidence of the soil foundation is so critical that the pipeline behaves as a simply supported beam carrying the loads imposed for the weight of the soil prism over the pipe and traffic loads.

Figure 29: Filled of the pipes to determine watertightness of the joint

Figure 30: Leaking Area.

Obviously, this new support configuration created a bending or flexure testing where the same lateral force (F) would induce compressive stresses on top of the specimen and tensile stresses at the bottom. Once initiated the application of the test force the specimen failed at a load of 3, 500 lbs. at which point the load dropped significantly, but then stabilized as shown in Figure 32.

Figure 31: The support near the joint was removed

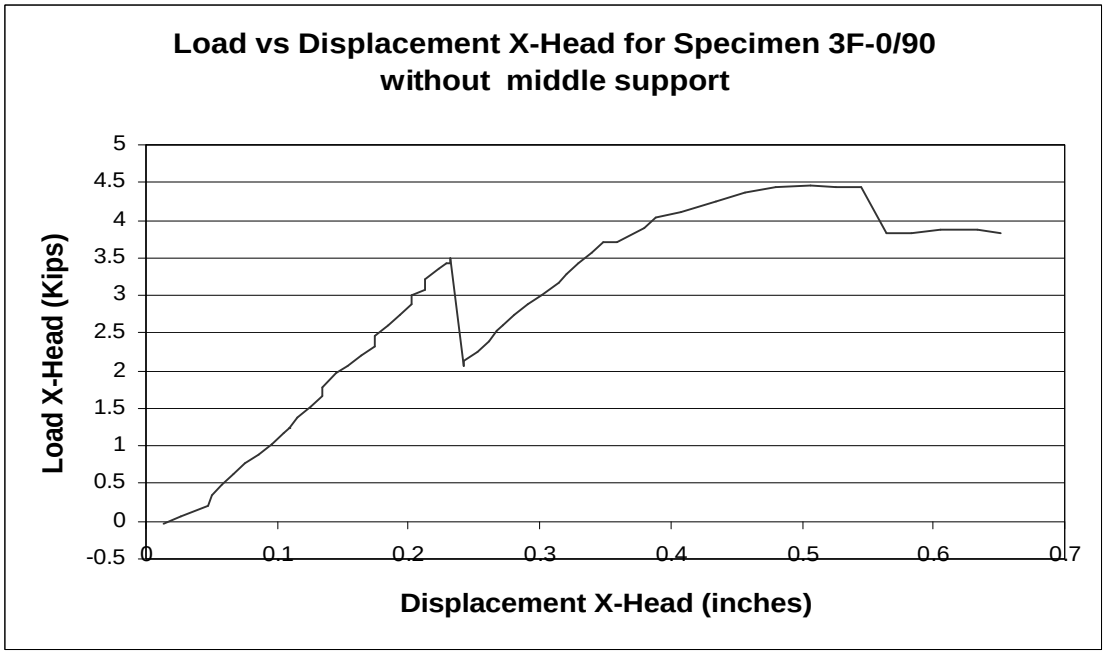

Figure 32: Load vs. Displacement X- Head for Specimen 3F – 0/90 without middle support

The pipe barrel cracked right by the cradle block used to transmit the shear force from the actuator to the pipe as shown in Figure 33. The Strain gauge oriented longitudinally on top of the pipe reported the largest reading corresponding to the strain resulted from the compressive bending stresses acting on top of the pipe because of the positive bending moment. Neither the FRP jacket nor the Hydro-Stone showed any signal of deterioration.

Figure 33: Mode of failure for Specimen 3F-0/90 after removing center support

Subsequently, the second specimen, 3F-45/45, was filled with water in order to determine the watertightness of the wrapped joint before the application of the test load (F). As noticed

with specimen 3F-0/90, water emerged from the border line in between the pipe and the Hydro-Stone immediately after the pipe was filled with water as pictured in Figure 34.

Figure 34: The Leak Emerges from the Interface in Between the Pipe and Hydro-stone

Later, the specimen was subjected to the test vertical load (F) in accordance with the established ASTM standard test procedure. Strain gauges attached to the FRP surface registered minute strain values that confirmed the fact that the shear stress induced across the joint was again, as in specimen 3F-0/90, supported by the bell-spigot joint and hydrostone rim. The magnitude of the vertical force (F) was insufficient to demand from the FRP any contribution of

additional strength than the provided by the pipe to support the differential load induced across the joint. Obviously, no visible indication of deterioration of the FRP jacket or Hydro-stone rim was present. Therefore, it was decided to reload the specimen to failure. Upon reloading it failed at 17 Kips. At this moment the pipe barrel cracked right by the timber support as shown in figure 35. Moderate strain values were measured over the FRP.

Figure 35: Failure Mode of Specimen 3F-45/45

CHAPTER 5

ANALYSIS OF RESULTS

The first part of this chapter is devoted to present and discuss the results obtained from the GPR survey. Following, results from the laboratory tests to determine the effectiveness of the FRP wrapping technique to repair a faulty pipe joint are reported and commented.

Ground Penetrating Radar Survey

During the GPR survey the antenna with a center frequency of 300 MHz exhibited significant attenuation of the radar signal with depth. Recognition of geological conditions or detection of features underground at a depth greater than 15 feet was impractical using the 300 MHz antenna. Therefore, only results obtained with the 80 MHz antenna are presented in this section.

The radar profile obtained along the grid line EW1 (above pipeline) using the 80 MHz antenna is shown in Figure 36 and 37. In the field, the GPR survey along the mentioned grid line was performed in a continuous base. Because of the extensive of the profile, it has been divided into two different figures. The graphic representation of the reflected radar signals shows clearly several anomalies along the surveyed area. First of all, two series of hyperbolic reflections represent two buried pipes oriented along the north-south direction, which is perpendicular to the surveyed grid line. Each series of hyperbolic reflections show clearly the top of the pipe (upper red stripe), the water way area (green stripe) and the bottom part of the pipe (second red stripe); the remaining hyperbolic bands are multiple reflections from the previous stripes.

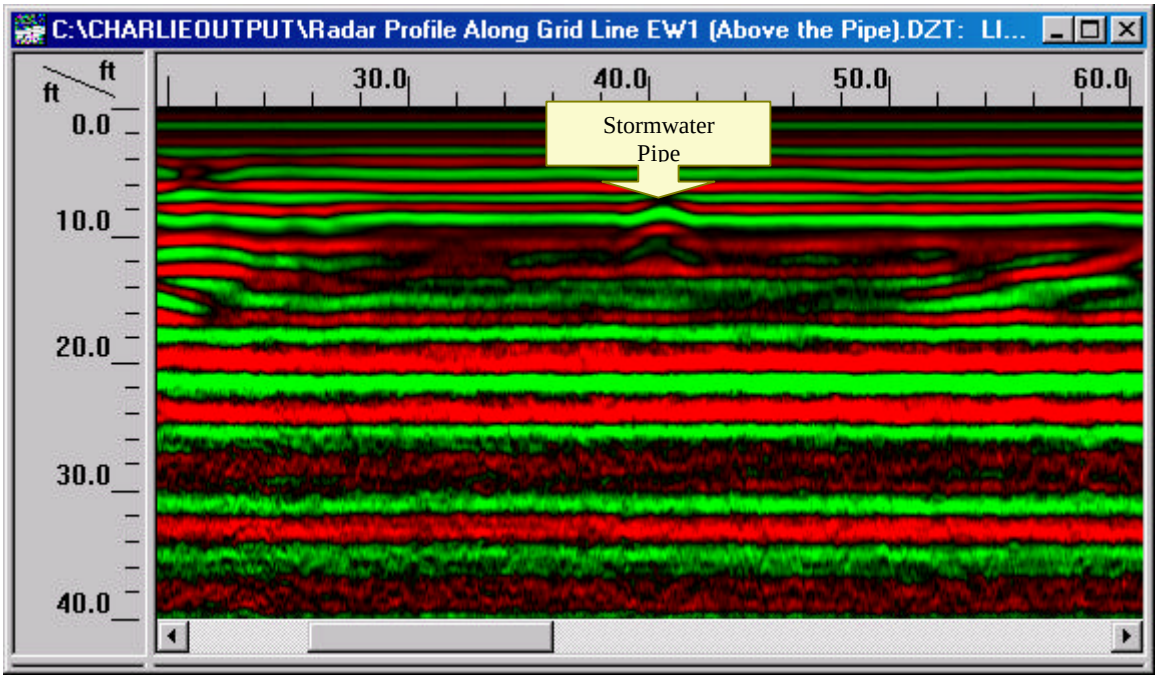

Figure 36: GPR Profile along grid line EW1 (Above Sewer Pipeline)

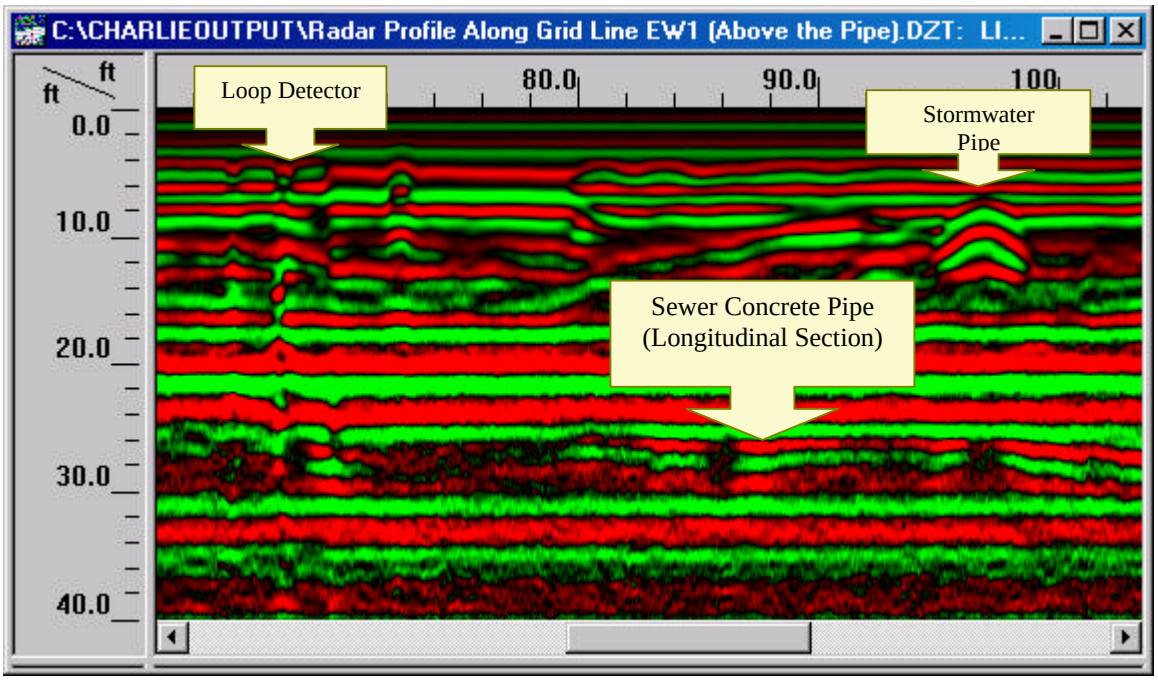

Figure 37: GPR Profile along grid line EW1 (Above Sewer Pipeline)

Other significant features in Figures 36 and 37 are the two discontinuities that irrupt in the uniform reflection patterns shown in the profile near the two stormwater pipes. As shown in the GPR profile, radar reflections describe certain uniformity along the 160-foot long survey in the upper mid part of the profile. This uniformity is interrupted in the area surrounding the pipes indicating a variation in the continuity of the soil stratigraphy. These irregularities can be the result of disturbances to the natural sedimentation of the soil caused by the construction activity involved during the emplacement of the stormwater pipes. A strong radar reflection is caused by a loop detector embedded in the pavement to control the semi-actuated traffic signals at the intersection as shown in Figure 37.

According to the profile in Figure 36 and Figure 37 at a depth of 20 feet a strong radar reflection is observed represented by several solid bands placed one on top of another. Those reflections are believed to be layers of sandy soil very uniform in thickness with a high content of moisture. The difference in color among the solid bands indicates the existence of different soil materials with particular dielectric constants (electrical properties) that respond differently to the pass of the electromagnetic waves. Bright colors correspond to high amplitude pulses, it means that there is a strong reflection (or a high dielectric constant); while dark colors correspond to low amplitude signals (or low dielectric constant). In Figures 36 y 37 the red bands are believed to be sandy soil with considerable percentage of fines capable of retain moisture, which confer to this material a larger dielectric constant (25-30) than the grey bands which are believed to be homogeneous coarse sandy soil deposits with a lower moisture content and a lower dielectric constant. The exaggerated uniformity in their thicknesses makes believe that they were placed in site over (as compacted backfill) and underneath (as bedding) of the sewer

concrete pipeline shown in the profile. The concrete pipeline is point up in the profile at a depth of 24 feet approximately. In this particular survey the depth indicated in the vertical scale of the image should not be taken as the exact elevation of the pipe from the ground surface since the velocity of the radar wave was calculated based on a theoretical dielectric value for sandy soils of 6 (SIRveyor SIR-20 user's manual, 2002). A better approximation of the depth might be obtained calculating the velocity of the radar waves for the site knowing the exact depth of a buried object. The pipeline image shows three irregular bands corresponding to the top, content and bottom of the pipe. The oscillational shape of the bands (radar reflections) is typical of pipes surveyed along their main axis. As observed in Figure 37 only part of the concrete pipe is represented in the profile since most of the radar signal attenuates with depth.

When using GPR a convincing evidence of the existence of a leakage (infiltration/exfiltration) in pipes are changes in the frequency of radar signals. In a colored profile as the presented herein, changes in the frequency are represented by suddenly changes in color in large uniform pattern. One of the advantages of RADAN in processing raw data is the existence of several standard display color tables that allow to perceive easily changes in the amplitude of the recorded radar signal. Therefore, the same profile obtained along the grid line EW1 (above pipeline) is now presented in Figure 38 and 39 using another color code to facilitate the perception of any change in color (variation in the amplitude of the radar signal) along the pipeline. These changes in the amplitude of radar signal are caused by changes in the dielectric constant of the transmitting medium, for instance, due to the presence of water from a leak along the pipeline.

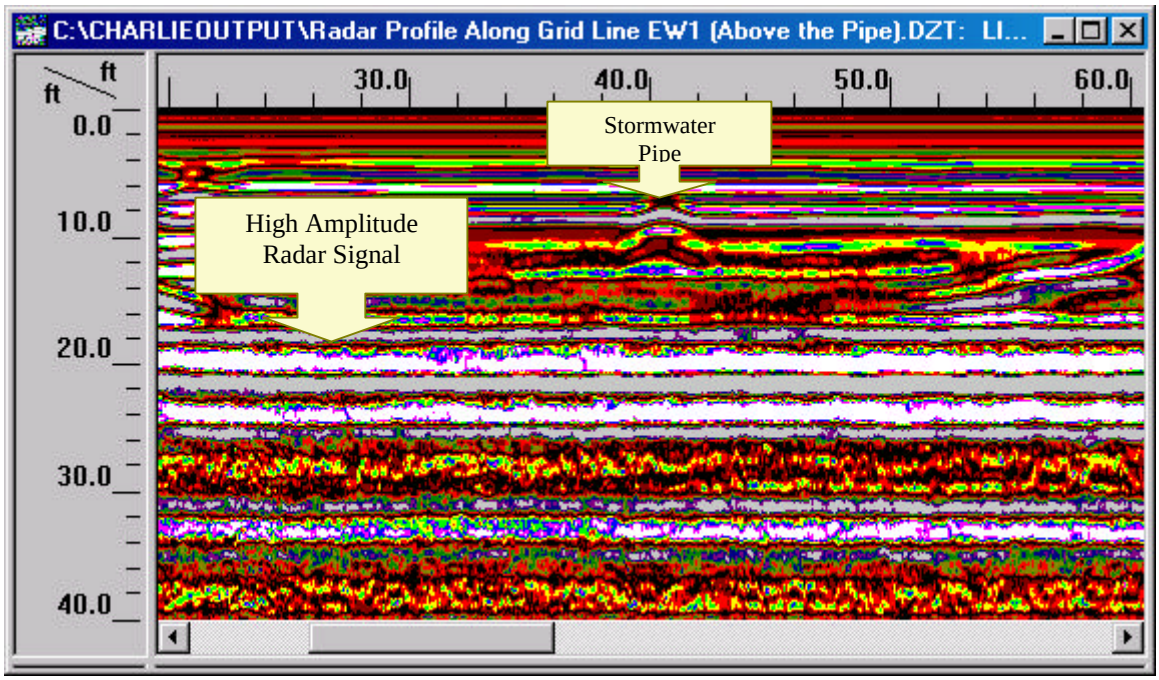

Figure 38: GPR Profile along grid line EW1 (Above Sewer Pipeline) using a different color code

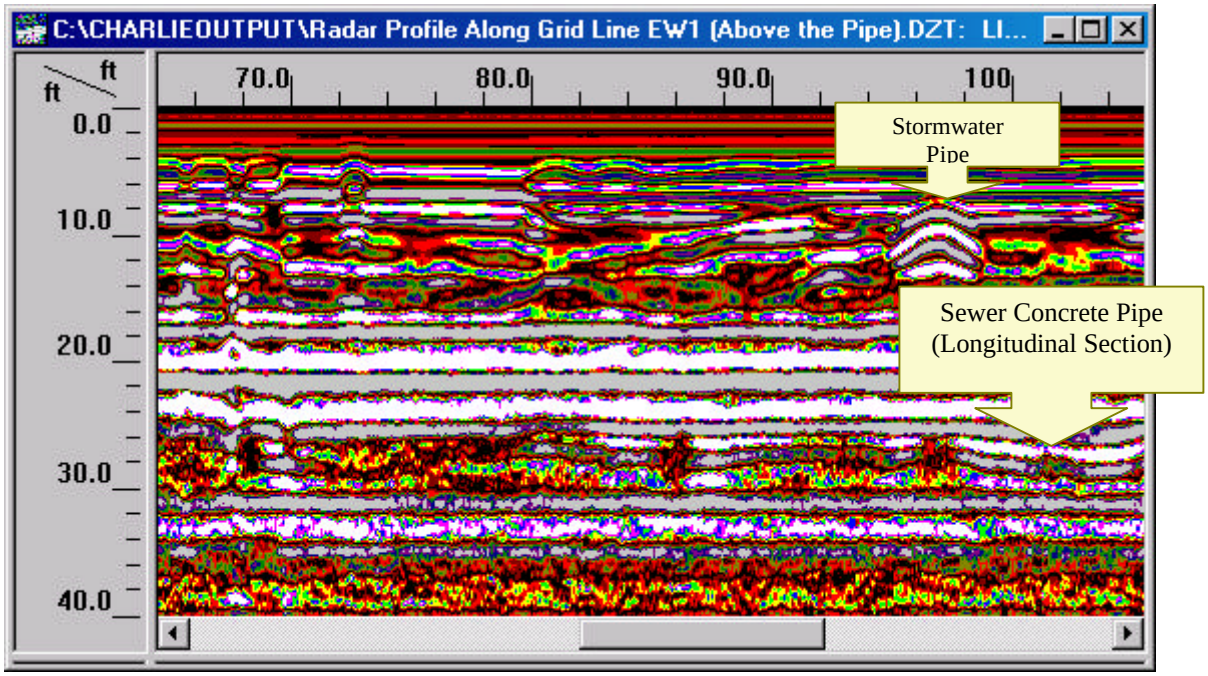

Figure 39: GPR Profile along grid line EW1 (Above Sewer Pipeline) using a different color code

As seen in Figure 39, the sewer pipeline is barely depicted because of the significant attenuation; nevertheless, it can be seen that there is not any significant change in the frequency of the radar signal (change in color) along the perceptible pipe segment suggesting that no leak is present at least along this short section.

Radar profiles obtained using the 80 MHz antenna are shown in Figures 40, 41, and 42 for survey lines perpendicular to the sewer pipe (only grid lines NS2, NS4 and NS8 are shown). In all these profiles significant attenuation of the radar signal with depth is observed.

Figure 40 was obtained out of the suspected area of the leak. As seen in the profile, no subsidence of the pavement surface is present on it. A small hyperbolic reflection is noticed at a depth of 12 feet at the left side of the figure, it corresponds to a concrete pipe placed parallel to the curve, which is believed to be a storm water pipe. Moreover, Figure 40 shows several inclined bands relatively uniform in thicknesses that correspond to strata with different electric behavior (dielectric constant) given the changes in color. The dark area seen in the lower part of the profile is believed to be a material with a low dielectric constant as a homogeneous sand deposit. No evidence of the sewer pipe is provided by the profile.

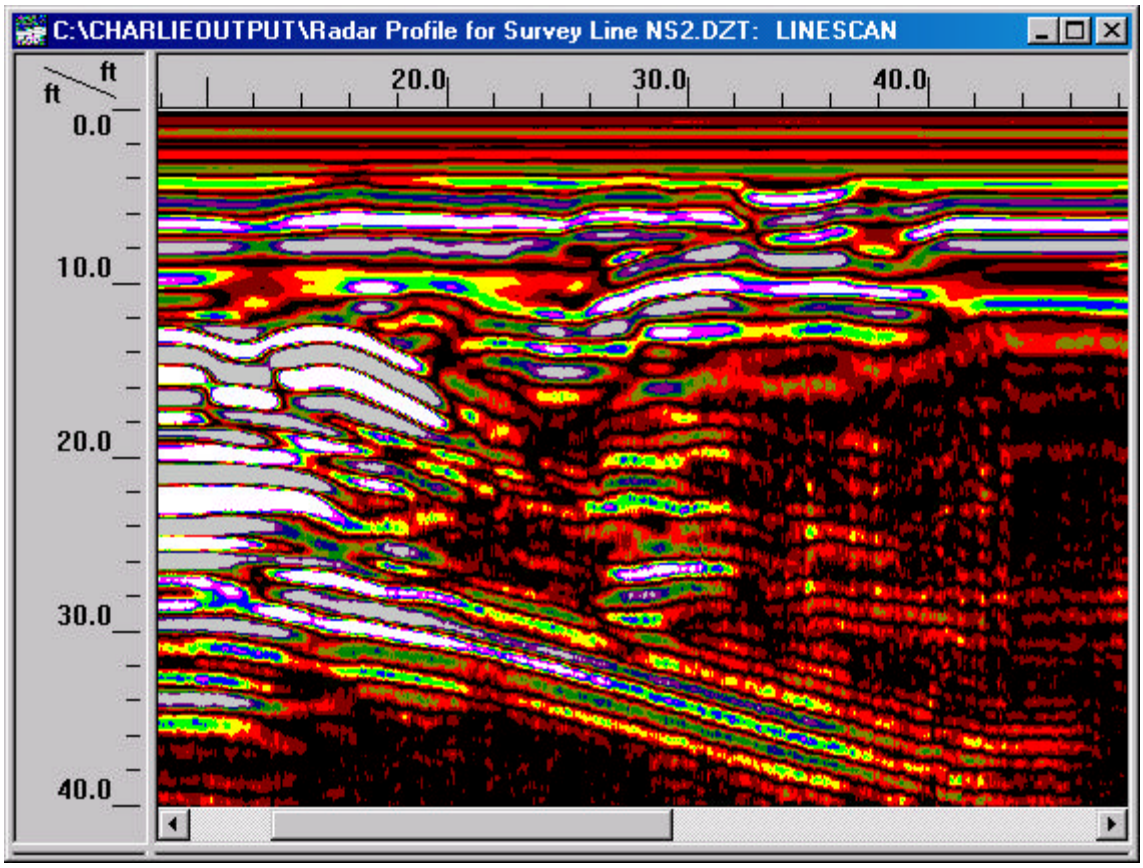

Figure 40: GPR profile along grid line NS2 obtained using 80MHz antenna

Figure 41 shows the radar profile obtained along the grid line NS4 located within the area where the pipe leak is suspected to be. In the upper part of the profile a noticeable subsidence of the pavement surface within the white marks is evident. Even two distinguishable layers from asphalt batching repairs can be seen over the pavement depression. The profile in Figure 41 appears very consistent in regarding of the subsurface information featured in the previous profile 40. The same inclined uniform bands and darken zone in the lower part of the profile make think the predominance of sandy soil underneath. As in others profiles obtained during the GPR survey the attenuation of the radar signal is present.

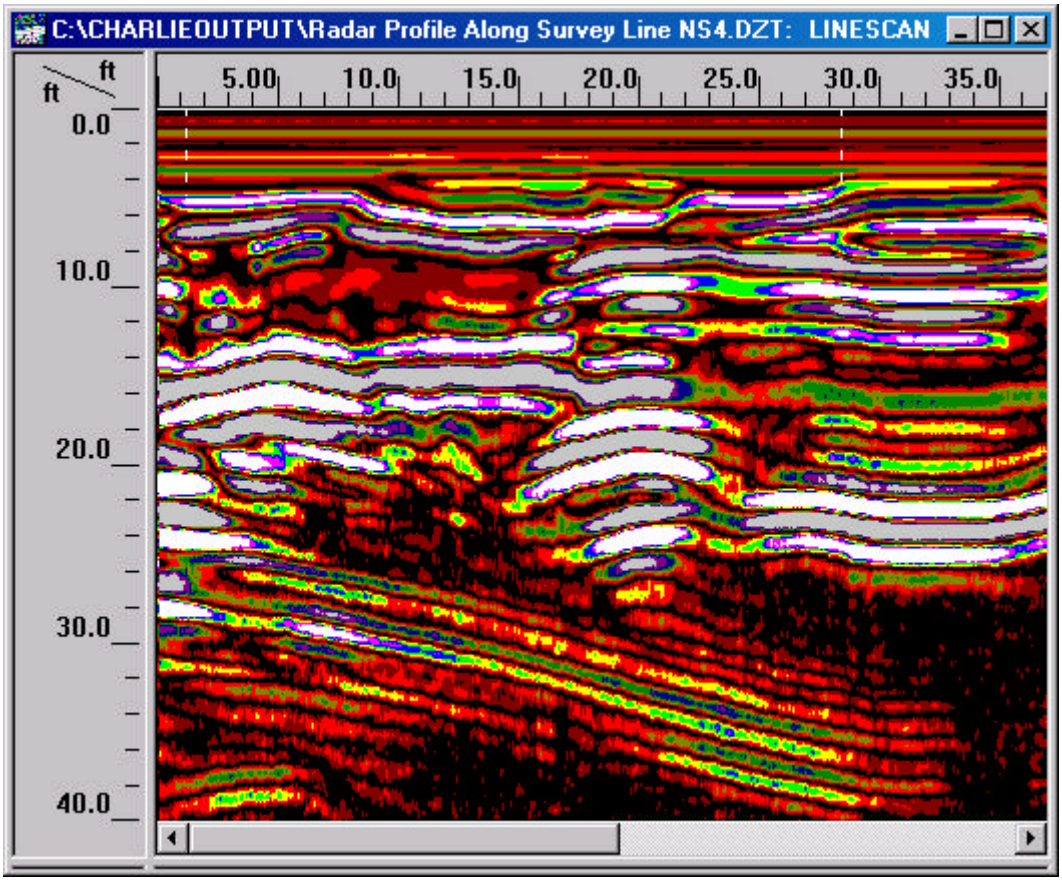

Figure 41: GPR profile along the grid line NS4 obtained using the 80MHz antenna

In Figure 42 a point reflection at a depth of 25 feet is believed to be the sewer pipe. Due to attenuation of the radar signal the hyperbolic shape is not fully displayed in the profile. The same point reflection signal was obtained in three other profiles confirming the existence of the concrete pipe. Since significant lost of signal occurs at the pipe depth, it is difficult to identify any anomaly around the sewer pipe. In order to facilitate the recognition of the radar reflection caused by the sewer pipe, the same profile along the grid line NS8 shown in Figure 42 has been depicted in Figure 43 using a different color code. No evidence of leakage is perceived from the mentioned profile across the pipe.

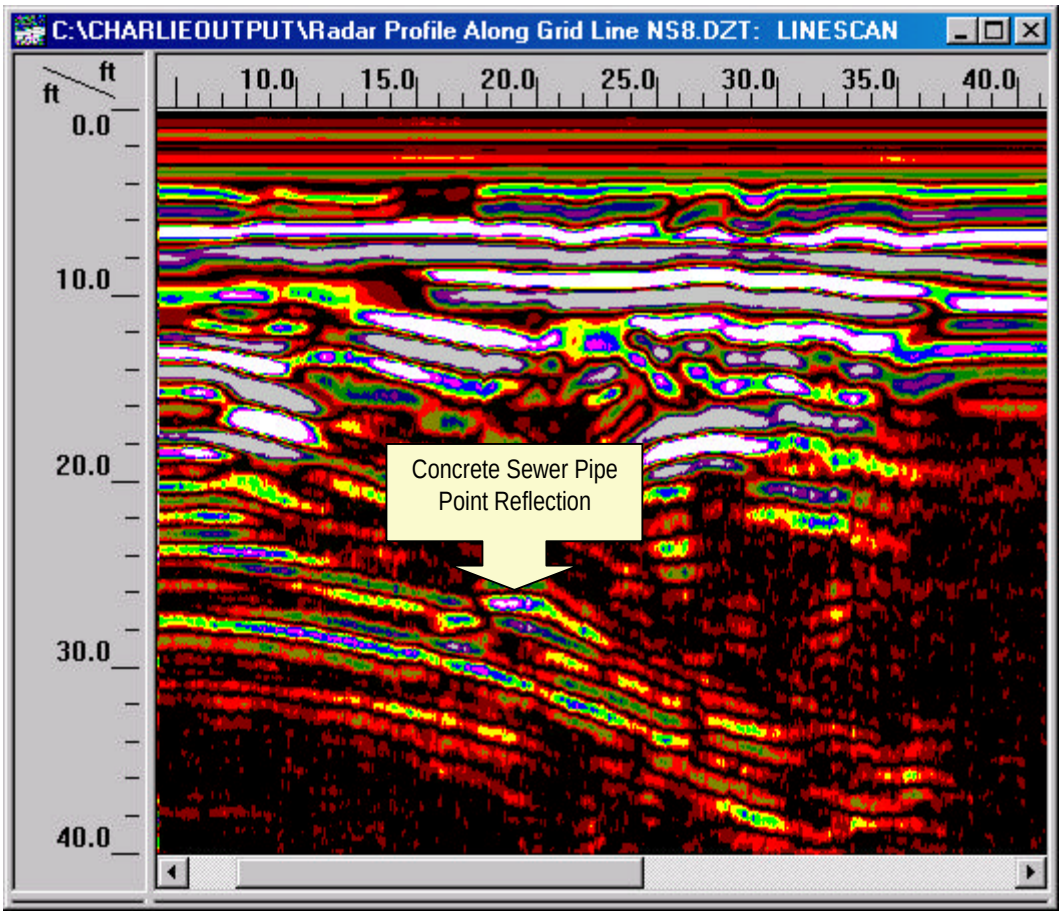

Figure 42: GPR profile along the grid line NS8 obtained using the 80MHz antenna.

It is important to mention that signal reflections generated by buried pipelines in other areas such as stormwater pipes on UCF campus and drainage pipelines at road side of University Boulevard as shown in Figure 44, were clearly detected. The latter makes to believe that the significant attenuation of the radar signal at the area of study is due to the extreme high conductivity of soils which have been severely contaminated by the leakage of sewage from the distressed sewer pipeline.

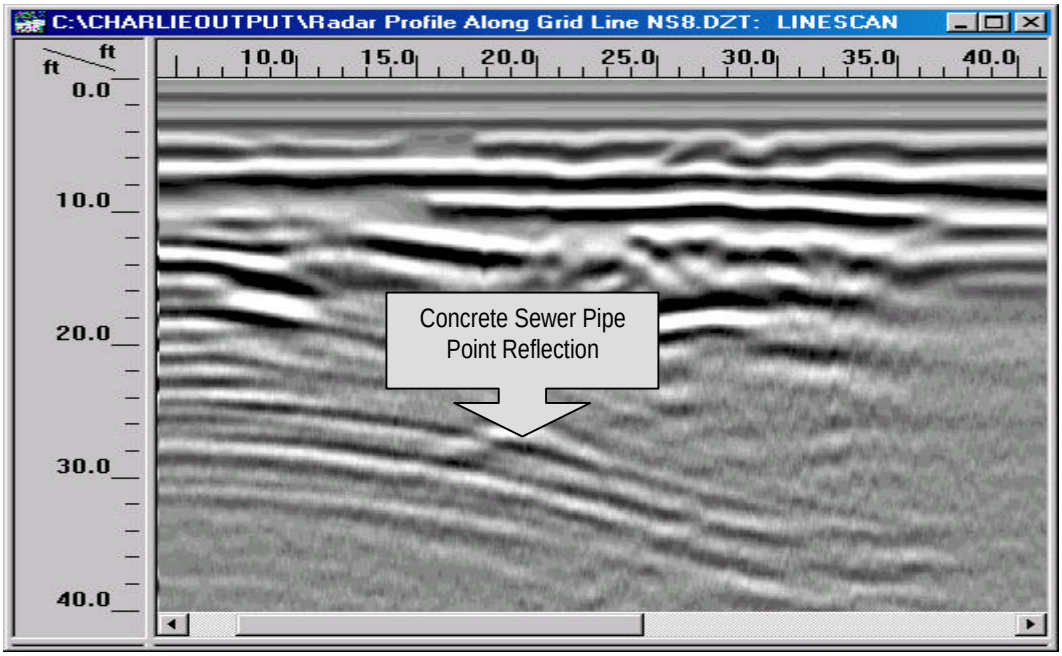

Figure 43: GPR profile along the grid line NS8 obtained using the 80 MHz antenna

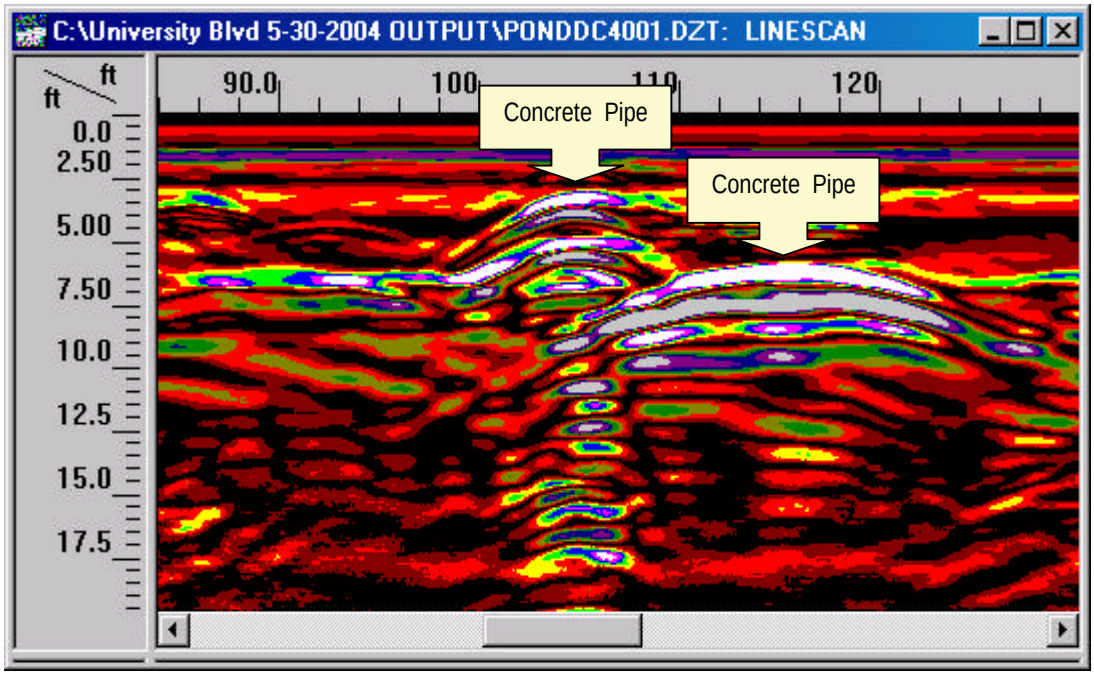

Figure 44: GPR profile from adjacent side of University Boulevard Westbound obtained using the 80 MHz antenna

Experimental Development of the Wrapping Repair Technique using FRP

In this section the results obtained from the laboratory testing are discussed separately for each one of the specimen. First, results from the static loading and watertight test of the specimen 3F-0/90 are commented. Then, a succinct analysis of the results for specimen 3F-45/45 during loading and watertight of the joint are presented.

Specimen 3F-0/90

Figure 44 shows the load-displacement curve depicted from actuator x-head for specimen 3F-0/90 for the support condition showed in Figure 28 in accordance with ASTM designation C497-03a. As observed in Figure 44 no sudden drop of the curve occurred during the loading procedure. The latter is an indication that the test force (F) did not exceeded the capacity of the pipe joint in resisting the differential load induced by the shear force (F). The load-displacement curve clearly depicts two well defined portions, one of them characterized by a moderate slope at the beginning of the curve and the other one marked by a steeper slope at the end. The flat portion corresponds to the compression of the rubber band attached to the support at the beginning of the loading while the steeper portion of the curve is the pipe barrel response to the test force (F).

All the strain gauges attached to the FRP reported negligible strains (less than 12 microstrains), this is an indication of the structural capacity of the hydro-stone rim and bell-spigot joint itself in resisting the vertical force (F).

In the additional test load to determine the ultimate strength of the repaired joint, in which the middle support was removed, specimen 3F-0/90 upon reloading failed at 3,500 lbs.

At this point the pipe barrel cracked since it no longer resists the deflection (bending) imposed for such a load. Therefore, the structural capacity of the repaired joint in resisting bending has exceeded the capacity of the pipe itself. It is important to mention that strains gauges over the FRP surface exhibited again negligible strain values since most of the stresses withstanding the bending effect are generated by the Hydro-stone rim . Based on the previous evaluation of the capacity of the repaired joint, it can be affirmed that the faulty joint has been effectively strengthened throughout the construction of the Hydro-stone jacket. The role of the FRP in the repair technique would be to hold together the hydro-stone rim once it failed (cracks) under the effect of significant external forces. At this point the FRP jacket becomes effective as a hoop tension band, and the only restrain against catastrophic failure

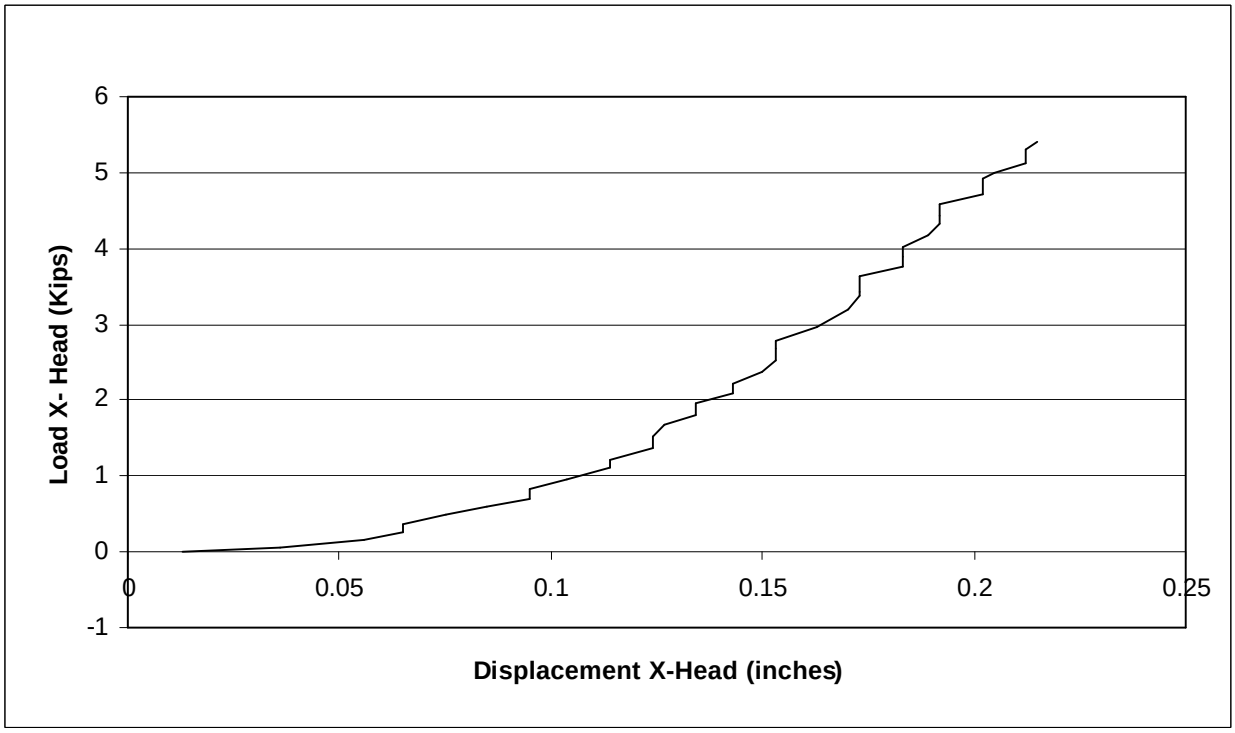

Figure 45: Load vs. Displacement X-head for Specimen 3F-0/90

The repair technique as conceived in this research visible failed in perpetrating the watertight condition of the joint. Materials used herein in the sealing of the bell-spigot joint prior to the casting of the Hydro-stone must be substituted. Instead, improved epoxy sealants must be used to guarantee the watertight condition. The Hydro-stone should not be thought as capable of stopping the infiltration/exfiltration (leakage) condition.

Specimen 3F-45/45

As mentioned in the previous chapter under “Test Observation”, for the second specimen, 3F-45/45, the watertight test was performed before loading of the specimen. Special interest arose in determining whether the loading of the specimen contributed in the formation of the leak at the pipe joint. Even before the application of the test load the pipe leaked at the joint. There is no doubt that the materials and procedure used in sealing the joint is ineffective, even though particular care was took during the sealing of the joint for this second specimen.

As experienced with specimen 3F-0/90, the specimen 3F-45/45 successfully resisted the application of the test force (F) of 5,600 lbs as calculated in accordance the ASTM procedure. No significant strains are registered across the FRP surface, the two-material structure; pipe and Hydro-stone rim are responsible in supporting the differential force induced by the application of the test load.

For the second loading test performed to specimen 3F-45/45, the specimen failed at a load of 17,000 lbs. At this point a loud noise was heard and the pipe barrel cracked failing in a tension mode. During the loading of the specimen strains were monitored over the FRP surface. Significant values were registered by the strain rosettes attached to the FRP as shown in Figure

45 leading to think that under the effect of this mayor vertical force (F) the FRP started providing some resistance against the loading. It was confirmed that the repaired joint exceeded the structural capacity of the pipe itself, demonstrating the effectiveness of the Hydro-stone rim in strengthening the faulty joint.

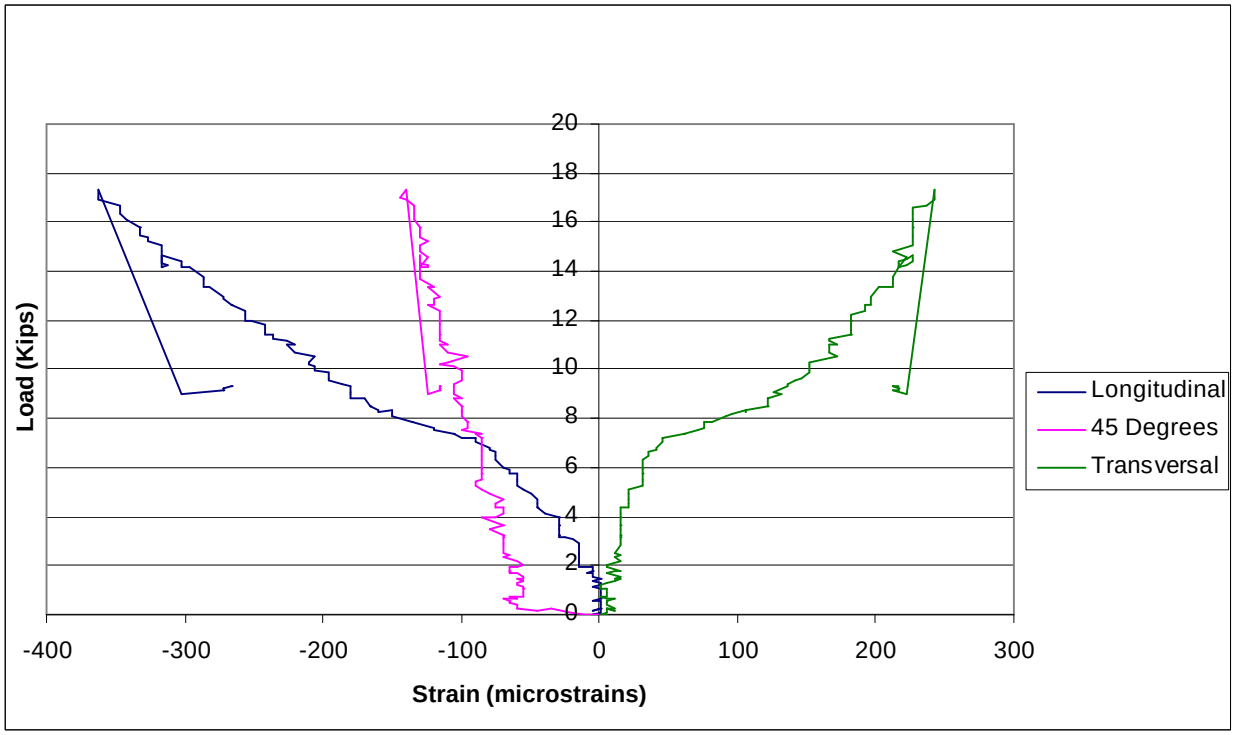

Figure 46: Strain Readings from Top of Specimen 3F-45/45 when Loaded to Failure

CHAPTER 6

SUMMARY AND CONCLUSIONS

An extensive ground penetrating radar survey was conducted in a roadway where noticeable subsidence of the pavement surface might be an indicative of the presence of a leaking pipe underneath. Two antennas with different center frequencies, 300 and 80 MHz were tested in order to get the most reliable information. The data acquisition was performed using the SIRveyor SIR-20 manufactured by GSSI and raw data processing using RADAN 5.0 multi-processing software.

The GPR survey was conducted over an area in which an imaginary grid of 160 feet by 48 feet was marked to facilitate the data collection. The survey grid enclosed an area over the suspected leakage and further away from it and survey lines were oriented parallel and perpendicular to the main axis of the sewer pipe. Three pilot studies were conducted to determine optimum data acquisition parameters at the area of study. Even though both antennas exhibited significant signal attenuation with depth, the 300 HMz antenna was not reported depths greater than 15 feet making it impractical for this research.

In detecting leaks underground along the sewer pipe, special observation was taken in sudden changes in large uniform patterns and changes in the frequency of the signal. The abrupt changes in uniform patterns have to do with disturbances to the natural stratigraphy of the soil material caused by an external agent as a joint leakage (infiltration/exfiltration). The changes in

the frequency or amplitude of the radar signal are caused by changes in the dielectric constant of the material (electric material property) medium due to the saturation by water from leakages. Besides the existence of voids around the pipeline constitutes evidence in the tracking of leaking pipes.

During the GPR survey performed in the area of study, no clear detection of the designated sewer concrete pipe was observed. This lack of traceable signal from the subsurface was the result of the significant attenuation of the radar signal with depth that made impossible to discern effectively any anomaly along the designated pipeline. Although different antennas having center frequencies of 300 and 80 MHz were used and a variety of settings on the GPR unit were tried, the buried pipeline was barely detectable. Nevertheless, signal reflections generated by buried pipelines in other areas such as stormwater pipes on UCF campus and drainage pipelines at road side of University Boulevard were clearly detected, which makes to believe that the significant attenuation of the radar signal at the area of study is due to the extreme high conductivity of soils which have been severely contaminated by the leakage of sewage from the distressed.

Is important to mention that the detection of any feature using GPR, including the detection of leakages, demands an elevated grade of expertise and training from the operator to interpret the information collected. Although advancing digital processing may help in refining and improving the results of the investigated matter, the judgment of the operator continues being of paramount importance in accomplishing the final results.

In developing a repair technique for strengthening faulty pipe joints, two major goals should be achieved. The first goal would be related to the idea of conceiving a technique that was

easily performed on the field with materials widely available in the construction market. The second goal would be sponsored by the idea of developing a repair technique capable of providing to the damaged joint with the strength necessary to carry the load imposed by the weight of filling material (overburden pressure), roadway traffic and even the load caused by internal fluid pressure. The first goal has been accomplished as can be seen in the "Materials and Test Preparation" sections of this thesis, whereas common materials and a simple installation procedure make this technique feasible from the installation point of view.

On the other hand, the results obtained from the loading experiments back up the second mayor goal of the repair technique. All the loading tests highlight the stiffness of the jacket formed by the Hydro-stone rim and the wrapped plies of carbon fiber reinforced composites. The Hydro-stone rim provided the repaired joint with the strength necessary in supporting the external load acting over the pipe joint and eventually the FRP would act as a hoop tension band holding the Gypsum material in one piece once it reaches it ultimate strength and rupture under the effect of any extraordinary load. However, the repair technique as conceived in this research visible failed in perpetrating the watertight condition of the joint. Materials used herein in the sealing of the bell-spigot joint prior to the casting of the Hydro-stone must be substituted. Instead, improved epoxy sealants should be used to guarantee the watertight condition. The Hydro-stone should not be thought as capable of stopping the infiltration/exfiltration (leakage) condition.

One of the aspects that remain to be demonstrated in further investigation is the number of FRP plies to be wrapped around the joint. As previously referred the number of FRP layers used in this research was three; however this number might be reduced making the technique even more cost-effective and less time consuming. In facilitating the wrapping task, the Hydro-

stone rim could be built in a circular shape instead of the octagonal it showed in this research. This circular shape not only would facilitate the application of the FRP but also avoid the stress concentration at the corner of the sides of the octagonal shape.

The initiative of this research was pioneering and its results were considered especially satisfactory. The technique and procedure developed in this study are believed to be unique according to the literature search consulted prior to the development of this project. The technique is under the planning of applying for a patent through UCF office of Sponsored Research.

APPENDIX

CALCULATION OF VERTICAL TEST FORCE, F

According to ASTM C497-03a, a vertical test force is applied on the suspended portion of the joint (spigot) until the total differential load , including the weight of a pipe, is 4000 pounds per foot of pipe diameter. Therefore, the specified reaction should be equal to:

$$R = 4{,}000\ lbs \times Diameter_{\text{int}\,ernal}\ (ft)$$
$$R = 4{,}000 \times 1.25$$
$$R = 5{,}000\ lbs$$

Since the pipes are unharnessed, and assuming nominal weight of the pipe, $W_p = (140\ lbs\ per\ foot) \times 8\ ft = 1{,}120\ lbs$

$$\sum M_A = 0 = (W_F \times ((OAL/2) - 2.75))) + (F \times L_F) - (R \times (OAL - 4.75))$$
$$\sum M_A = 0 = (W_p \times 47) + (F \times 75.20) - (R \times 94.75)$$
$$F = \frac{(R \times 94.75) - (W_p \times 47)}{75.20}$$
$$F = \frac{(5{,}000 \times 94.75) - (1{,}120 \times 47)}{75.20}$$
$$\boxed{F = 5{,}599.87 \approx 5{,}600\ lbs}$$

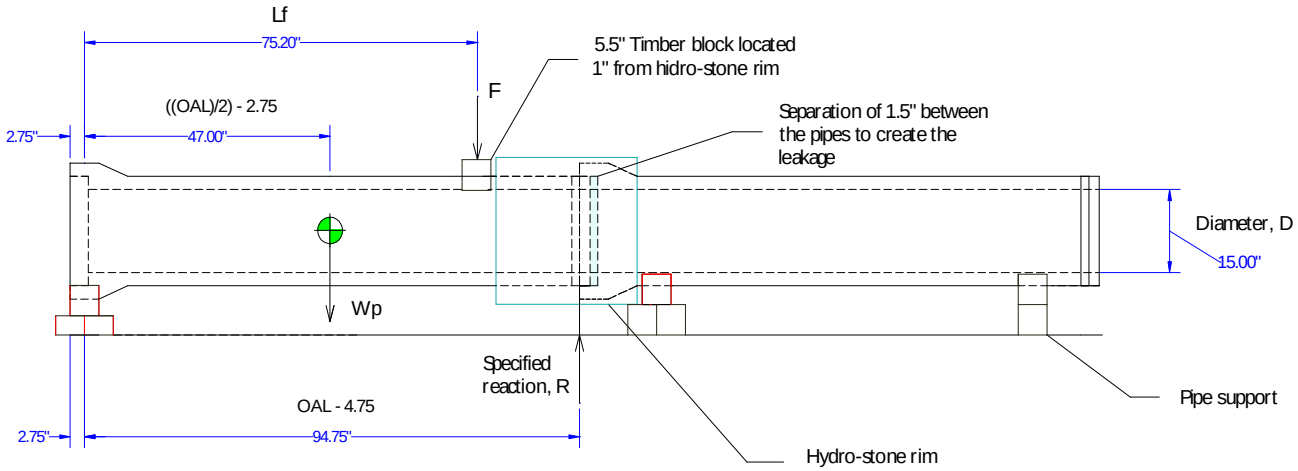

OAL=Overall length
F =Additional test force
R =Test requirement
Wp =Nominal weight of test pipe

REFERENCES

Spangler, M. G., & Handy, R. L. (1982). Soil Engineering. New York: Harper & Row, Publishers, Inc.

Saadatmanesh, H., Ehsani, M. R., & Li, M. W. (1994). Strength and ductility of concrete columns externally reinforced with fiber composite straps. ACI Structural Journal, July- August 1994, 434 – 47.

Eiswirth, M., Heske, C., Burn, L.S., & DeSilva, D. (2001). New Methods for Water Pipe Assessment: Proceedings of IWA 2. World Water Congress, 15-19 Oct 2002. Berlin, Germany.

Graf, Fred L. (1986). Radar Leak Pinpointing: Proceedings of International Conference on Radar. Nanjing, China.

Powers M.H., and Olhoeft G.R. (1997) Modeling the GPR Response of Leaking Buried Pipes, pp. 525.

Osama, H., & Giamou, P. (1998). Ground-Penetrating Radar for Detection of Leaks in Buried Plastic Water Distribution Pipes: Proceedings of the seventh international conference on ground-penetrating radar. Lawrence, Kansas, USA.

Eyuboglu, S., Mahdi,H. & Al-Shukri, H. (2003). Detection of Water Leaks Using Ground Penetrating Radar.

Kuo, S. S. Publications and Presentations available FTP: //people.cecs.ucf.edu/kuo/

Conyers, L. B., Ernenwein, E. G., & Bedal, L. A. (2002). Ground penetrating radar (GPR) mapping as a method por planning excavation strategies, Petra, Jordan. Available FTP: //e-tiquity.saa.org/~etiquity/1/index.html

Thomas, J., & St. John, T. (2003, January). FRP Technology Repairs and Strengthening Municipal Aqueduct System. PublicWorks

Quakewrap, Inc. (2002). Quakewrap Fabrics Technical Data Sheet. Online. Available FTP: //www.quakewrap.com/fabrics.htm

Quakewrap, Inc. (2002). QuakeBond Resins Technical Data Sheet. Online. Available FTP: //www.quakewrap.com/resins.htm

Tang, B. (1997) Fiber Reinforced Polymer Composites Applications in USA DOT-Federal Highway Administration: Proceedings of the first Korea/U.S.A. Road Workshop.

Pico, O. (1997). Confinement Effectiveness of Square FRP Tubes in Hybrid Columns. Thesis, University of Central Florida, Orlando.

Geophysical Survey Systems and Inc, (2003) Radan for Windows Version 5.0 User's Manual pp 11.

Geophysical Survey Systems and Inc, (2002) SIRveyor SIR-20 User's Manual pp 45.

ASTM International. Designation: C 497-03a: Standard Test Methods for Concrete Pipes, Manhole Sections or Tile. pp 9.